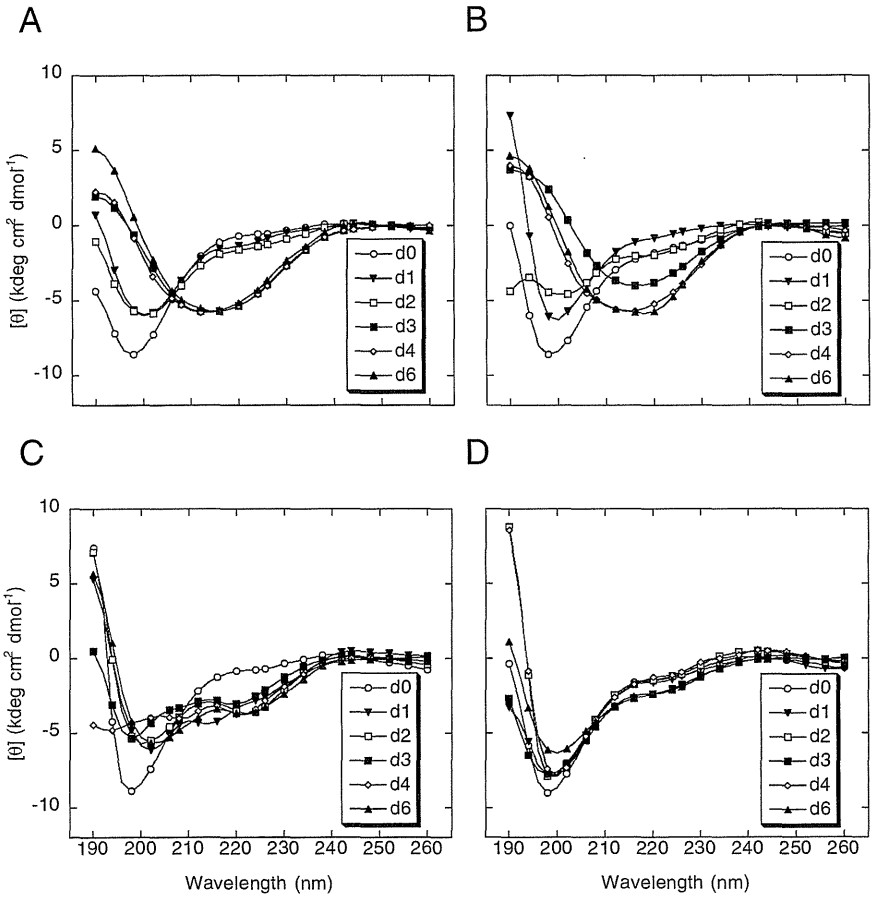

Fig. 6. α-Synuclein (αS) secondary structure dynamics. (A–D) 35 μM αS were incubated at 37 °C for 6 days in 20 mM Tris buffer, pH 7.4, in buffer alone (A) or in the presence of 250 μM trihexyphenidyl hydrochloride (Tri) (B), or 25 μM (C), or 250 μM melatonin (Mel) (D). Spectra were acquired immediately at the start of the incubation period, Day 0 (○), and after Days 1 (▼), 2 (□), 3 (□), 4 (◇), and 6 (▲). The spectra presented at each time are representative of those obtained during each of 3 independent experiments.

When αS alone was immediately added to the primary mixed neurons of mesencephalon and neostriatum, its cell viability was not significantly different from Mel only or buffer only (controls) (Fig. 7). The viability of cells with Mel-treated αS was also not significantly different from that of the controls. However, incubation of αS for 2 days, during which time oligomers, protofibrils, and fibril would be formed, produced aggregates that were significantly more toxic. Viability of cells with untreated αS was approximately 70%. Treatment of αS with Mel increased cell viability to approximately 86%, which was a highly significant increase relative to αS alone ($p < 0.01$) (Fig. 7). The same qualitative relationships among these experimental groups were observed after 6 days of incubation. Viability of cells with untreated αS was approximately 83%, which was significantly less toxic than that with αS after 2 days incubation ($p < 0.05$). Treatment of αS with Mel significantly increased cell viability to approximately 97% ($p < 0.01$) (Fig. 7).

4. Discussion

Mel is normally synthesized and secreted during the dark phase of the day. A primary function of Mel secretion is to convey information about daily cycles of light and darkness to body physiology (Srinivasan et al., 2005). A substantial body of evidence suggests that Mel may inhibit fibril formation by a variety of amyloidogenic proteins (Srinivasan et al., 2005). Aβ studies showed that Mel strongly inhibited the spontaneous formation of β-sheets and Aβ fibrils (Pappolla et al., 1998). The protective actions of Mel against Aβ neurotoxicity have been repeatedly confirmed (Poeggeler et al., 2001; Shen et al., 2002a, 2002b, 2002c). Furthermore, Mel inhibited the expected time-dependent elevation of Aβ in a transgenic mouse model of Alzheimer's amyloidosis (Matsubara et al., 2003).

Mel has been shown to attenuate arsenite-induced apoptosis via a reduction of aggregated αS levels in rat brain (Lin et al., 2007) by Western blot analysis. Similarly, Ishido reported that Mel inhibits maneb-induced assembly of αS in

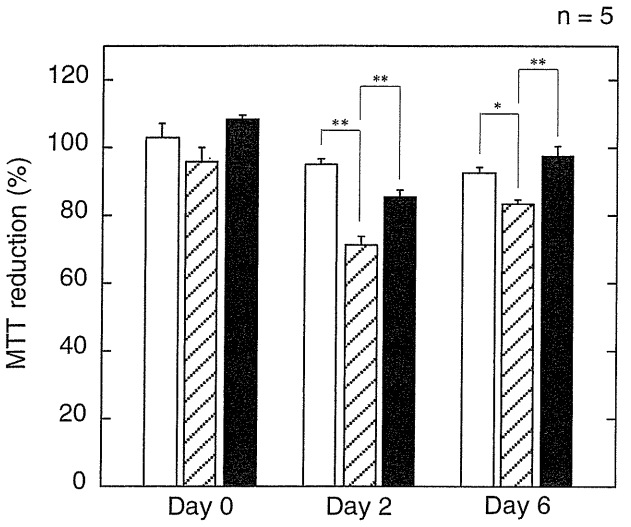

Fig. 7. 3-[4,5-dimethylthiazol-2-yl]-2,5-diphenyltetrazolium bromide (MTT) metabolism. α-Synuclein (αS) was incubated with or without melatonin (Mel) in 10 mM Tris, pH 7.4, at 37 °C for 0, 2, and 6 days prior to addition to primary mixed neurons comprised of mesencephalon and neostriatum. Effects of Mel only (open bars), untreated αS (cross-hatched bars), and Mel-treated αS (closed bars) on cell metabolism were determined fluorometrically using MTT 48 hours after sample addition. Each bar represents mean ± standard error. Statistical significance among groups was determined using 1-way fractional analysis of variance (ANOVA) and multiple comparison tests. Differences reaching statistical significance are noted by line segments between samples, along with their associated p values, where * signifies $p < 0.05$ and ** signifies $p < 0.01$.

rat pheochromocytoma cells investigated by immunostaining (Ishido, 2007). Thus, it is reasonable that Mel has an anti-misfolding effect for αS as well as for Aβ. We sought here to examine more deeply the mechanism of inhibition, a goal critical to accelerating knowledge-based strategies for inhibitor targeting and design.

We began by studying fibril formation in parallel with assessing assembly β-sheet content. EM and ThS experiments revealed that Mel strongly inhibited β-sheet and fibril formation by αS. Working backwards systematically along the αS assembly pathway, we found that Mel also was a highly effective inhibitor of protofibril formation and peptide oligomerization.

Some studies have sought to establish the relative importance of different types of αS assemblies in disease pathogenesis (for a recent review, see Caughey and Lansbury, 2003). For example, protofibrils have been linked to an A30P form of early-onset PD (Conway et al., 1998). Protofibrils forming annular structures may have pore-like properties and might damage membranes (Lashuel et al., 2002; Volles et al., 2001). A linear association/annealing of these spherical species, resembling an Aβ protofibril, was observed in the preparation of protofibrils (Conway et al., 2000). Morphology of void volume fraction gained by our SEC experiments was consistent with this report. The area of this fraction displayed monotonic increase until plateau with the incubation. Taken together, our data suggested that Mel strongly inhibits the protofibril formation. Thus, the ability of Mel to inhibit both fibril and protofibril formation suggests that it may be of value for therapeutic strategies targeting these 2 assembly types.

Most recently, new studies have revealed that low-order oligomeric forms of αS are also toxic and critical species (Outeiro et al., 2008; Paleologou et al., 2009; Tsigelny et al., 2008). Outeiro et al. have shown that formation of dimeric and oligomeric αS species, both of which are thought to precede the formation of larger intracellular inclusions, are central steps toward cytotoxicity which can be targeted through the activity of molecular chaperones, such as heat shock protein 70 (Hsp70) (Outeiro et al., 2008). Consistent with this result, toxicity is seen without heavily aggregated αS, and it has been suggested that soluble species mediate toxicity (Xu et al., 2002). It was reported that soluble spheroid oligomer has 1.5–3.0 nm in height by AFM studies (Apetri et al., 2006), being consistent with our results of AFM. Very recently, it was reported that αS exists physiologically as a helically folded tetramer that precedes αS misfolding and aggregation, suggesting that stabilization of the tetramer could reduce LBD pathogenicity (Bartels et al., 2011).

Recently, annular αS oligomers have been isolated from human brain samples of MSA (Pountney et al., 2004). A novel enzyme-linked immunosorbent assay (ELISA) method revealed an elevation of αS oligomer level in plasma samples obtained from PD patients compared with controls (El-Agnaf et al., 2006), and the levels of soluble oligomers of αS were higher in the DLB brain than in the brain of patients with Alzheimer's disease and the controls (Paleologou et al., 2009), which support the idea that oligomers are the toxic species. Interestingly, EC50 of Mel for the oligomerization of αS was 2.7 μM (compound:peptide ratios of 1 to approximately 26), suggesting that Mel especially has strong inhibitory effect on oligomerization of αS. The strong ability of Mel to block formation of low-order αS oligomers in our results suggests that it might also be of value for targeting what some have argued are the proximate neurotoxins in LBD (Outeiro et al., 2008; Paleologou et al., 2009; Tsigelny et al., 2008).

Our CD studies, in concert with ThS experiments, showed that Mel produced a conformer population comprising primarily statistical coils. Whether Mel stabilizes unfolded αS conformers or destabilizes folded conformers or oligomeric or fibrillar assemblies cannot be ascertained from the data extant. However, the consequences of Mel treatment in the αS system do appear to differ from those observed in certain other inhibitor:amyloidogenic protein systems. For example, Zhu et al. (2004) reported that the flavonoid baicalein stabilized a partially folded conformer of αS that existed within oligomeric assemblies. Conway et al. (2001) showed that dopamine or levodopa inhibits the fibrillization of αS filaments, presumably through stabiliza-

tion of αS into protofibrillar structures unable to form fibrils. Taniguchi et al. (2005) reported the formation of tau oligomers in the presence of phenothiazines, polyphenols, or porphyrins. In each of these cases, the inhibitors stabilized oligomeric states in which the respective protein maintained at least a partial fold. The ability of Mel to block αS monomer folding and, especially, oligomerization thus is a particularly important aspect of a mechanism underlying its effect.

The most important biological consequence of αS association is the production of neurotoxic assemblies. In the work reported here, assemblies of αS that were added to cultures of primary neurons caused significant cellular damage, as measured by effects on MTT metabolism. There are some reports that the increase of cell viability in MTT assay was consistent with the increase of tyrosine hydroxylase activity in the cells of mesencephalon (Nobre-Júnior et al., 2009) and neostriatum (Barrachina et al., 2003). Our results that nonaggregated αS is less toxic than aggregated αS as well as that intermediate aggregates are more toxic than final aggregates were not inconsistent with reports that early intermediates of αS are toxic and critical species (Outeiro et al., 2008; Paleologou et al., 2009; Tsigelny et al., 2008). Mel substantially reduced these toxic effects after pretreatment of αS during assembly. Cellular injury caused by αS-mediated perturbation of cellular redox reactions is an important proposed disease mechanism in LBD (George et al., 2009). Prior studies have shown that Mel exhibits substantial antioxidant properties (Kotler et al., 1998; Reiter et al., 1997) so that Mel has been proposed as a potential therapeutic agent in diseases in which oxidative stress is thought to be a major pathogenic factor. There is 1 opposite report that melatonin is not always neuroprotective using the rotenone model of PD (Tapias et al., 2009). However, as shown in this report, Mel dose-dependently inhibits all steps of αS assembly process. Moreover, cell culture experiments with primary neurons suggested that Mel-treated αS assemblies might be less toxic than intact αS assemblies. Thus, it may be reasonable to speculate that Mel could delay the development of LBD, not only through scavenging reactive oxygen species, but also through directly inhibiting the assembly of αS in the brain.

The concentrations of Mel are in the low nanomolar range in the blood of human. As far as cerebrospinal fluid (CSF) is concerned, peak Mel concentrations ranged from 94 to 355 pm in human (Bruce et al., 1991; Reiter, 1991). The effective concentrations of Mel for αS assembly in our experiment may be somewhat higher compared with physiological levels of Mel in the brain. However, Mel exhibited antiassembly effects at substoichiometric concentration in all steps of αS assembly process, especially oligomerization. As Mel readily crosses the blood-brain barrier, Mel may exhibit antiassembly activities in vivo when administered in high doses and for a long time.

In conclusion, our demonstration here of the potent inhibitory effects of Mel on αS assembly, coupled with previously reported redox-based protective and ameliorative effects of Mel, suggest that Mel is worthy of consideration as a therapeutic agent for LBD.

Disclosure statement

The authors disclose no conflicts of interest.

Acknowledgements

We acknowledge the support of a grant for the Knowledge Cluster Initiative (High-Tech Sensing and Knowledge Handling Technology [Brain Technology]) (MY), a grant to the Amyloidosis Research Committee from the Ministry of Health, Labor, and Welfare, Japan (MY and KO), Kanae Foundation for the Promotion of Medical Science (KO), Alumni Association of the Department of Medicine at Showa University (KO), and Nagao Memorial fund (KO). Support from the Jim Easton Consortium for Alzheimer's Drug Discovery and Biomarkers at UCLA (DBT) is also acknowledged.

Appendix A. Supplementary data

Supplementary data associated with this article can be found, in the online version, at doi:10.1016/j.neurobiolaging.2011.10.015.

References

Abe, K., Saito, H., 1998. Amyloid β protein inhibits cellular MTT reduction not by suppression of mitochondrial succinate dehydrogenase but by acceleration of MTT formazan exocytosis in cultured rat cortical astrocytes. Neurosci. Res. 31, 295–305.

Apetri, M.M., Maiti, N.C., Zagorski, M.G., Carey, P.R., Anderson, V.E., 2006. Secondary structure of α-synuclein oligomers: characterization by raman and atomic force microscopy. J. Mol. Biol. 355, 63–71.

Baba, M., Nakajo, S., Tu, P.H., Tomita, T., Nakaya, K., Lee, V.M., Trojanowski, J.Q., Iwatsubo, T., 1998. Aggregation of α-synuclein in Lewy bodies of sporadic Parkinson's disease and dementia with Lewy bodies. Am. J. Pathol. 152, 879–884.

Barrachina, M., Domínguez, I., Ambrosio, S., Secades, J., Lozano, R., Ferrer, I., 2003. Neuroprotective effect of citicoline in 6-hydroxydopamine-lesioned rats and in 6-hydroxydopamine-treated SH-SY5Y human neuroblastoma cells. J. Neurol. Sci. 215, 105–110.

Bartels, T., Choi, J.G., Selkoe, D.J., 2011. α-Synuclein occurs physiologically as a helically folded tetramer that resists aggregation. Nature 477, 107–110.

Bitan, G., Lomakin, A., Teplow, D.B., 2001. Amyloid β-protein oligomerization: prenucleation interactions revealed by photo-induced cross-linking of unmodified proteins. J. Biol. Chem. 276, 35176–35184.

Bitan, G., Teplow, D.B., 2004. Rapid photochemical cross-linking—a new tool for studies of metastable, amyloidogenic protein assemblies. Acc. Chem. Res. 37, 357–364.

Bruce, J., Tamarkin, L., Riedel, C., Markey, S., Oldfield, E., 1991. Sequential cerebrospinal fluid and plasma sampling in humans: 24-hour melatonin measurements in normal subjects and after peripheral sympathectomy. J. Clin. Endocrinol. Metab. 72, 819–823.

Caughey, B., Lansbury, P.T., 2003. Protofibrils, pores, fibrils, and neurodegeneration: separating the responsible protein aggregates from the innocent bystanders. Annu. Rev. Neurosci. 26, 267–298.

Conway, K.A., Harper, J.D., Lansbury, P.T., 1998. Accelerated in vitro fibril formation by a mutant α-synuclein linked to early-onset Parkinson disease. Nat. Med. 4, 1318–1320.

Conway, K.A., Harper, J.D., Lansbury, P.T., Jr., 2000. Fibrils formed in vitro from α-synuclein and two mutant forms linked to Parkinson's disease are typical amyloid. Biochemistry 39, 2552–2563.

Conway, K.A., Rochet, J.C., Bieganski, R.M., Lansbury, P.T., Jr., 2001. Kinetic stabilization of the α-synuclein protofibril by a dopamine-α-synuclein adduct. Science 294, 1346–1349.

El-Agnaf, O.M., Salem, S.A., Paleologou, K.E., Curran, M.D., Gibson, M.J., Court, J.A., Schlossmacher, M.G., Allsop, D., 2006. Detection of oligomeric forms of α-synuclein protein in human plasma as a potential biomarker for Parkinson's disease. FASEB J. 20, 419–425.

Evans, K.C., Berger, E.P., Cho, C.G., Weisgraber, K.H., Lansbury, P.T., Jr., 1995. Apolipoprotein E is a kinetic but not a thermodynamic inhibitor of amyloid formation: implications for the pathogenesis and treatment of Alzheimer disease. Proc. Natl. Acad. Sci. U. S. A. 92, 763–767.

Fancy, D.A., Kodadek, T., 1999. Chemistry for the analysis of protein–protein interactions: rapid and efficient cross-linking triggered by long wavelength light. Proc. Natl. Acad. Sci. U. S. A. 96, 6020–6024.

Feany, M.B., Bender, W.W., 2000. A Drosophila model of Parkinson's disease. Nature 404, 394–398.

Forno, L.S., 1996. Neuropathology of Parkinson's disease. J. Neuropathol. Exp. Neurol. 55, 259–272.

Gai, W.P., Power, J.H., Blumbergs, P.C., Blessing, W.W., 1998. Multiple-system atrophy: a new α-synuclein disease? Lancet 352, 547–548.

George, J.L., Mok, S., Moses, D., Wilkins, S., Bush, A.I., Cherny, R.A., Finkelstein, D.I., 2009. Targeting the progression of Parkinson's disease. Curr. Neuropharmacol. 7, 9–36.

Giasson, B.I., Duda, J.E., Quinn, S.M., Zhang, B., Trojanowski, J.Q., Lee, V.M., 2002. Neuronal α-synucleinopathy with severe movement disorder in mice expressing A53T human α-synuclein. Neuron 34, 521–533.

Gilman, S., Low, P.A., Quinn, N., Albanese, A., Ben-Shlomo, Y., Fowler, C.J., Kaufmann, H., Klockgether, T., Lang, A.E., Lantos, P.L., Litvan, I., Mathias, C.J., Oliver, E., Robertson, D., Schatz, I., Wenning, G.K., 1999. Consensus statement on the diagnosis of multiple system atrophy. J. Neurol. Sci. 163, 94–98.

Goedert, M., 2001. Parkinson's disease and other α-synucleinopathies. Clin. Chem. Lab. Med. 39, 308–312.

Goto, K., Mochizuki, H., Hattori, T., Nakamura, N., Mizuno, Y., 1997. Neurotoxic effects of papaverine, tetrahydropapaverine and dimethoxyphenylethylamine on dopaminergic neurons in ventral mesencephalic-striatal co-culture. Brain Res. 754, 260–268.

Ishido, M., 2007. Melatonin inhibits maneb-induced aggregation of α-synuclein in rat pheochromocytoma cells. J. Pineal Res. 42, 125–130.

Kotler, M., Rodríguez, C., Sáinz, R.M., Antolín, I., Menéndez-Peláez, A., 1998. Melatonin increases gene expression for antioxidant enzymes in rat brain cortex. J. Pineal Res. 24, 83–89.

Lashuel, H.A., Petre, B.M., Wall, J., Simon, M., Nowak, R.J., Walz, T., Lansbury, P.T., Jr., 2002. α-synuclein, especially the Parkinson's disease-associated mutants, forms pore-like annular and tubular protofibrils. J. Mol. Biol. 322, 1089–1102.

Lee, M.K., Stirling, W., Xu, Y., Xu, X., Qui, D., Mandir, A.S., Dawson, T.M., Copeland, N.G., Jenkins, N.A., Price, D.L., 2002. Human alpha-synuclein-harboring familial Parkinson's disease-linked Ala-53 –> Thr mutation causes neurodegenerative disease with alpha-synuclein aggregation in transgenic mice. Proc. Natl. Acad. Sci. U. S. A. 99, 8968–8973.

LeVine, H., 3rd, 1993. Thioflavine T interaction with synthetic Alzheimer's disease β-amyloid peptides: detection of amyloid aggregation in solution. Protein Sci. 2, 404–410.

LeVine, H., 3rd, 1999. Quantification of β-sheet amyloid fibril structures with thioflavin T. Methods Enzymol. 309, 274–284.

Li, H.T., Lin, X.J., Xie, Y.Y., Hu, H.Y., 2006. The early events of α-synuclein oligomerization revealed by photo-induced cross-linking. Protein Pept. Lett. 13, 385–390.

Li, J., Zhu, M., Rajamani, S., Uversky, V.N., Fink, A.L., 2004. Rifampicin inhibits α-synuclein fibrillation and disaggregates fibrils. Chem. Biol. 11, 1513–1521.

Lin, A.M., Fang, S.F., Chao, P.L., Yang, C.H., 2007. Melatonin attenuates arsenite-induced apoptosis in rat brain: involvement of mitochondrial and endoplasmic reticulum pathways and aggregation of α-synuclein. J. Pineal Res. 43, 163–171.

López-Burillo, S., Tan, D.X., Mayo, J.C., Sainz, R.M., Manchester, L.C., Reiter, R.J., 2003. Melatonin, xanthurenic acid, resveratrol, EGCG, vitamin C and α-lipoic acid differentially reduce oxidative DNA damage induced by Fenton reagents: a study of their individual and synergistic actions. J. Pineal Res. 34, 269–277.

Matsubara, E., Bryant-Thomas, T., Pacheco Quinto, J., Henry, T.L., Poeggeler, B., Herbert, D., Cruz-Sanchez, F., Chyan, Y.J., Smith, M.A., Perry, G., Shoji, M., Abe, K., Leone, A., Grundke-Ikbal, I., Wilson, G.L., Ghiso, J., Williams, C., Refolo, L.M., Pappolla, M.A., Chain, D.G., Neria, E., 2003. Melatonin increases survival and inhibits oxidative and amyloid pathology in a transgenic model of Alzheimer's disease. J. Neurochem. 85, 1101–1108.

McKeith, I.G., Dickson, D.W., Lowe, J., Emre, M., O'Brien, J.T., Feldman, H., Cummings, J., Duda, J.E., Lippa, C., Perry, E.K., Aarsland, D., Arai, H., Ballard, C.G., Boeve, B., Burn, D.J., Costa, D., Del Ser, T., Dubois, B., Galasko, D., Gauthier, S., Goetz, C.G., Gomez-Tortosa, E., Halliday, G., Hansen, L.A., Hardy, J., Iwatsubo, T., Kalaria, R.N., Kaufer, D., Kenny, R.A., Korczyn, A., Kosaka, K., Lee, V.M., Lees, A., Litvan, I., Londos, E., Lopez, O.L., Minoshima, S., Mizuno, Y., Molina, J.A., Mukaetova-Ladinska, E.B., Pasquier, F., Perry, R.H., Schulz, J.B., Trojanowski, J.Q., Yamada, M., Consortium on DLB, 2005. Diagnosis and management of dementia with Lewy bodies: third report of the DLB Consortium. Neurology 65, 1863–1872.

Mochizuki, H., Nakamura, N., Nishi, K., Mizuno, Y., 1994. Apoptosis is induced by 1-methyl-4-phenylpyridinium ion (MPP+) in ventral mesencephalic-striatal co-culture in rat. Neurosci. Lett. 170, 191–194.

Naiki, H., Nakakuki, K., 1996. First-order kinetic model of Alzheimer's β-amyloid fibril extension in vitro. Lab. Invest. 74, 374–383.

Nobre-Júnior, H.V., Oliveira, R.A., Maia, F.D., Nogueira, M.A., de Moraes, M.O., Bandeira, M.A., Andrade, G.M., Viana, G.S., 2009. Neuroprotective effects of chalcones from Myracrodruon urundeuva on 6-hydroxydopamine-induced cytotoxicity in rat mesencephalic cells. Neurochem. Res. 34, 1066–1075.

Ono, K., Hirohata, M., Yamada, M., 2007. Anti-fibrillogenic and fibril-destabilizing activities of anti-Parkinsonian agents for α-synuclein fibrils in vitro. J. Neurosci. Res. 85, 1547–1557.

Ono, K., Yamada, M., 2006. Antioxidant compounds have potent anti-fibrillogenic and fibril-destabilizing effects for α-synuclein fibrils in vitro. J. Neurochem. 97, 105–115.

Outeiro, T.F., Putcha, P., Tetzlaff, J.E., Spoelgen, R., Koker, M., Carvalho, F., Hyman, B.T., McLean, P.J., 2008. Formation of toxic oligomeric α-synuclein species in living cells. PLoS One 3, e1867.

Paleologou, K.E., Kragh, C.L., Mann, D.M., Salem, S.A., Al-Shami, R., Allsop, D., Hassan, A.H., Jensen, P.H., El-Agnaf, O.M., 2009. Detection of elevated levels of soluble α-synuclein oligomers in post-mortem brain extracts from patients with dementia with Lewy bodies. Brain 132, 1093–1101.

Pappolla, M., Bozner, P., Soto, C., Shao, H., Robakis, N.K., Zagorski, M., Frangione, B., Ghiso, J., 1998. Inhibition of Alzheimer β-fibrillogenesis by melatonin. J. Biol. Chem. 273, 7185–7188.

Pévet, P., Agez, L., Bothorel, B., Saboureau, M., Gauer, F., Laurent, V., Masson-Pévet, M., 2006. Melatonin in the multi-oscillatory mammalian circadian world. Chronobiol. Int. 23, 39–51.

Poeggeler, B., Miravalle, L., Zagorski, M.G., Wisniewski, T., Chyan, Y.J., Zhang, Y., Shao, H., Bryant-Thomas, T., Vidal, R., Frangione, B., Ghiso, J., Pappolla, M.A., 2001. Melatonin reverses the profibrillogenic activity of apolipoprotein E4 on the Alzheimer amyloid Aβ peptide. Biochemistry 40, 14995–15001.

Pountney, D.L., Lowe, R., Quilty, M., Vickers, J.C., Voelcker, N.H., Gai, W.P., 2004. Annular α-synuclein species from purified multiple system atrophy inclusions. J. Neurochem. 90, 502–512.

Reiter, R., Tang, L., Garcia, J.J., Muñoz-Hoyos, A., 1997. Pharmacological actions of melatonin in oxygen radical pathophysiology. Life Sci. 60, 2255–2271.

Reiter, R.J., 1991. Pineal melatonin: cell biology of its synthesis and of its physiological interactions. Endocr. Rev. 12, 151–180.

Shen, Y.X., Wei, W., Xu, S.Y., 2002a. Protective effects of melatonin on cortico-hippocampal neurotoxicity induced by amyloid β-peptide 25–35. Acta Pharmacol. Sin. 23, 71–76.

Shen, Y.X., Xu, S.Y., Wei, W., Sun, X.X., Liu, L.H., Yang, J., Dong, C., 2002b. The protective effects of melatonin from oxidative damage induced by amyloid β-peptide 25–35 in middle-aged rats. J. Pineal Res. 32, 85–89.

Shen, Y.X., Xu, S.Y., Wei, W., Wang, X.L., Wang, H., Sun, X., 2002c. Melatonin blocks rat hippocampal neuronal apoptosis induced by amyloid β-peptide 25–35. J. Pineal Res. 32, 163–167.

Spillantini, M.G., Crowther, R.A., Jakes, R., Cairns, N.J., Lantos, P.L., Goedert, M., 1998. Filamentous α-synuclein inclusions link multiple system atrophy with Parkinson's disease and dementia with Lewy bodies. Neurosci. Lett. 251, 205–208.

Srinivasan, V., Pandi-Perumal, S.R., Maestroni, G.J., Esquifino, A.I., Hardeland, R., Cardinali, D.P., 2005. Role of melatonin in neurodegenerative diseases. Neurotox. Res. 7, 293–318.

Storch, A., Hwang, Y.I., Gearhart, D.A., Beach, J.W., Neafsey, E.J., Collins, M.A., Schwarz, J., 2004. Dopamine transporter-mediated cytotoxicity of β-carbolinium derivatives related to Parkinson's disease: relationship to transporter-dependent uptake. J. Neurochem. 89, 685–694.

Taniguchi, S., Suzuki, N., Masuda, M., Hisanaga, S., Iwatsubo, T., Goedert, M., Hasegawa, M., 2005. Inhibition of heparin-induced tau filament formation by phenothiazines, polyphenols, and porphyrins. J. Biol. Chem. 280, 7614–7623.

Tapias, V., Cannon, J.R., Greenamyre, J.T., 2009. Melatonin treatment potentiates neurodegeneration in a rat rotenone Parkinson's disease model. J. Neurosci. Res. 88, 420–427.

Tsigelny, I.F., Crews, L., Desplats, P., Shaked, G.M., Sharikov, Y., Mizuno, H., Spencer, B., Rockenstein, E., Trejo, M., Platoshyn, O., Yuan, J.X., Masliah, E., 2008. Mechanisms of hybrid oligomer formation in the pathogenesis of combined Alzheimer's and Parkinson's diseases. PLoS One 3, e3135.

Volles, M.J., Lansbury, P.T., Jr., 2003. Zeroing in on the pathogenic form of α-synuclein and its mechanism of neurotoxicity in Parkinson's disease. Biochemistry 42, 7871–7878.

Volles, M.J., Lee, S.J., Rochet, J.C., Shtilerman, M.D., Ding, T.T., Kessler, J.C., Lansbury, P.T., Jr., 2001. Vesicle permeabilization by protofibrillar α-synuclein: implications for the pathogenesis and treatment of Parkinson's disease. Biochemistry 40, 7812–7819.

Wood, S.J., Wypych, J., Steavenson, S., Louis, J.C., Citron, M., Biere, A.L., 1999. α-synuclein fibrillogenesis is nucleation-dependent. Implications for the pathogenesis of Parkinson's disease. J. Biol. Chem. 274, 19509–19512.

Xu, J., Kao, S.Y., Lee, F.J., Song, W., Jin, L.W., Yankner, B.A., 2002. Dopamine-dependent neurotoxicity of α-synuclein: a mechanism for selective neurodegeneration in Parkinson disease. Nat. Med. 8, 600–606.

Yazawa, I., Giasson, B.I., Sasaki, R., Zhang, B., Joyce, S., Uryu, K., Trojanowski, J.Q., Lee, V.M., 2005. Mouse model of multiple system atrophy α-synuclein expression in oligodendrocytes causes glial and neuronal degeneration. Neuron 45, 847–859.

Zhu, M., Rajamani, S., Kaylor, J., Han, S., Zhou, F., Fink, A.L., 2004. The flavonoid baicalein inhibits fibrillation of α-synuclein and disaggregates existing fibrils. J. Biol. Chem. 279, 26846–26857.

doi:10.1093/brain/awr348 Brain 2012: 135; 833–846 | 833

BRAIN
A JOURNAL OF NEUROLOGY

Non-human primate model of amyotrophic lateral sclerosis with cytoplasmic mislocalization of TDP-43

Azusa Uchida,[1] Hiroki Sasaguri,[1] Nobuyuki Kimura,[2] Mio Tajiri,[1] Takuya Ohkubo,[1] Fumiko Ono,[3] Fumika Sakaue,[1] Kazuaki Kanai,[4] Takashi Hirai,[5] Tatsuhiko Sano,[1] Kazumoto Shibuya,[4] Masaki Kobayashi,[1] Mariko Yamamoto,[1] Shigefumi Yokota,[1] Takayuki Kubodera,[1] Masaki Tomori,[5] Kyohei Sakaki,[5] Mitsuhiro Enomoto,[5] Yukihiko Hirai,[6] Jiro Kumagai,[7] Yasuhiro Yasutomi,[2] Hideki Mochizuki,[8] Satoshi Kuwabara,[4] Toshiki Uchihara,[9] Hidehiro Mizusawa[1] and Takanori Yokota[1]

1 Department of Neurology and Neurological Science, Graduate School of Medicine, Tokyo Medical and Dental University, Tokyo 113-8519, Japan
2 Tsukuba Primate Research Centre, National Institute of Biomedical Innovation, Tsukuba 305-0843, Japan
3 Corporation for Production and Research of Laboratory Primates, Tsukuba 305-0843, Japan
4 Department of Neurology, Graduate School of Medicine, Chiba University, Chiba 260-8670, Japan
5 Department of Orthopaedic Surgery, Graduate School of Medicine, Tokyo Medical and Dental University, Tokyo 113-8519, Japan
6 Department of Biochemistry and Molecular Biology, Nippon Medical School, Tokyo 113-8602, Japan
7 Department of Pathology, Graduate School of Medicine, Tokyo Medical and Dental University, Tokyo 113-8519, Japan
8 Department of Neurology, Kitasato University School of Medicine, Kanagawa 228-8555, Japan
9 Laboratory of Structural Neuropathology, Tokyo Metropolitan Institute of Medical Science, Tokyo 156-8506, Japan

Correspondence to: Takanori Yokota,
Department of Neurology and Neurological Science,
Graduate School of Medicine,
Tokyo Medical and Dental University,
Bunkyo-ku, Tokyo 113-8519,
Japan
E-mail: tak-yokota.nuro@tmd.ac.jp

Amyotrophic lateral sclerosis is a fatal neurodegenerative disease characterized by progressive motoneuron loss. Redistribution of transactive response deoxyribonucleic acid-binding protein 43 from the nucleus to the cytoplasm and the presence of cystatin C-positive Bunina bodies are considered pathological hallmarks of amyotrophic lateral sclerosis, but their significance has not been fully elucidated. Since all reported rodent transgenic models using wild-type transactive response deoxyribonucleic acid-binding protein 43 failed to recapitulate these features, we expected a species difference and aimed to make a non-human primate model of amyotrophic lateral sclerosis. We overexpressed wild-type human transactive response deoxyribonucleic acid-binding protein 43 in spinal cords of cynomolgus monkeys and rats by injecting adeno-associated virus vector into the cervical cord, and examined the phenotype using behavioural, electrophysiological, neuropathological and biochemical analyses. These monkeys developed progressive motor weakness and muscle atrophy with fasciculation in distal hand muscles first. They also showed regional cytoplasmic transactive response deoxyribonucleic acid-binding protein 43 mislocalization with loss of nuclear transactive response deoxyribonucleic acid-binding protein 43 staining in the lateral nuclear group of spinal cord innervating distal hand muscles and cystatin C-positive cytoplasmic aggregates, reminiscent of the spinal cord pathology of patients with amyotrophic lateral sclerosis. Transactive response deoxyribonucleic acid-binding protein 43 mislocalization was

Received July 27, 2011. Revised October 26, 2011. Accepted November 14, 2011. Advance Access publication January 17, 2012

an early or presymptomatic event and was later associated with neuron loss. These findings suggest that the transactive response deoxyribonucleic acid-binding protein 43 mislocalization leads to α-motoneuron degeneration. Furthermore, truncation of transactive response deoxyribonucleic acid-binding protein 43 was not a prerequisite for motoneuronal degeneration, and phosphorylation of transactive response deoxyribonucleic acid-binding protein 43 occurred after degeneration had begun. In contrast, similarly prepared rat models expressed transactive response deoxyribonucleic acid-binding protein 43 only in the nucleus of motoneurons. There is thus a species difference in transactive response deoxyribonucleic acid-binding protein 43 pathology, and our monkey model recapitulates amyotrophic lateral sclerosis pathology to a greater extent than rodent models, providing a valuable tool for studying the pathogenesis of sporadic amyotrophic lateral sclerosis.

Keywords: TDP-43; Bunina bodies; cystatin C; cynomolgus monkeys; amyotrophic lateral sclerosis

Abbreviations: AAV = adeno-associated virus; ALS = amyotrophic lateral sclerosis; FTLD = frontotemporal lobar degeneration; HEK = human embryonic kidney; TDP-43 = transactive response DNA-binding protein 43

Introduction

Amyotrophic lateral sclerosis (ALS), also known as Lou Gehrig's disease, is an incurable progressive neurodegenerative disease characterized by muscle weakness and atrophy resulting from the combined loss of upper and lower motoneurons. Most cases of ALS are sporadic, and only 10% of ALS cases are of a familial form. Protein aggregates are one histopathological characteristic of ALS. A breakthrough in understanding ALS pathogenesis was the discovery of the 43-kDa transactive response DNA-binding protein (TDP-43), which was recently identified as the major component of the protein aggregates and of the insoluble fraction in the brains of patients with sporadic ALS and frontotemporal lobar degeneration (FTLD) (Arai *et al.*, 2006; Neumann *et al.*, 2006). TDP-43 is now expected to play an essential role in the pathogenesis of sporadic ALS, possibly equivalent to that of tau and beta amyloid in Alzheimer's disease or α-synuclein in Parkinson's disease.

Human TDP-43 is a highly conserved and ubiquitously expressed 414 amino acid nuclear protein that binds to both DNA and RNA (Ou *et al.*, 1995; Buratti *et al.*, 2001). In normal settings, TDP-43 is a primarily nuclear protein that functions in transcription regulation, alternative splicing and RNA stabilization (Buratti *et al.*, 2008), as well as in microRNA metabolism (Buratti *et al.*, 2010). Pathological TDP-43 can be abnormally truncated, phosphorylated and ubiquitinated, and most TDP-43 is mislocalized from the nucleus to the cytoplasm or neurites (Arai *et al.*, 2006; Neumann *et al.*, 2006). Of note, almost all neurons with cytoplasmic TDP-43 accumulations show a dramatic depletion of normal nuclear TDP-43. Thus, both gain and loss of functions are potential disease mechanisms, either due to the loss of normal nuclear TDP-43 expression, or cytoplasmic mislocalization (Arai *et al.*, 2006; Neumann *et al.*, 2006; Cairns *et al.*, 2007). Therefore, cytoplasmic TDP-43 mislocalization with loss of its nuclear staining is a key feature found in the majority of patients' brains and spinal cords (Arai *et al.*, 2006; Neumann *et al.*, 2006).

TDP-43 strictly regulates its messenger RNA levels by directly binding to an intron in the 3′-untranslated region of its own transcript and enhancing its splicing (Ayala *et al.*, 2010; Polymenidou *et al.*, 2011), however, the expression level of TDP-43 can be upregulated ~1.5-fold (Mishra *et al.*, 2007; Gitcho *et al.*, 2009) in FTLD/ALS. Moreover, mutations in the *TDP-43* gene are associated with familial ALS (Kabashi *et al.*, 2008; Yokoseki *et al.*, 2008), in which TDP-43 is also frequently mislocalized within motoneurons of the spinal cord. These reports support the hypothesis that mislocalization of this protein plays a central role in the disease pathogenesis. The rodent, *Drosophila*, *Ceanorhabditis elegans* and zebrafish models with overexpressed mutant as well as wild-type TDP-43 show severe motor symptoms and wild-type TDP-43 localizes exclusively or primarily to nuclei (Ash *et al.*, 2010; Hanson *et al.*, 2010; Kabashi *et al.*, 2010; Li *et al.*, 2010; Shan *et al.*, 2010; Voigt *et al.*, 2010; Wils *et al.*, 2010; Xu *et al.*, 2010; Swarup *et al.*, 2011), although mutant TDP-43 is more likely to accumulate in the cytoplasm (Swarup *et al.*, 2011). The results of the rodent models suggested that overexpressed nuclear wild-type TDP-43 is toxic, but provide little insight for the significance of mislocalized wild-type TDP-43. Even in mouse models that overexpress wild-type TDP-43 with mutated nuclear localization signals, total human and mouse nuclear TDP-43 was not reduced (Igaz *et al.*, 2011) when compared with that in littermate wild-type controls. Together, these reported mouse models might have a different TDP-43 pathology from that found in patients with ALS. Expecting that a primate model of ALS might more closely reflect the TDP-43 pathology in human patients with ALS, we overexpressed human wild-type TDP-43 in the spinal motoneurons of a non-human primate, the cynomolgus monkey, using an adeno-associated virus (AAV) 1 vector.

Materials and methods

Human subjects

Neurologists clinically diagnosed ALS with the aid of electrophysiological examinations. The clinical diagnosis of definite ALS was based on El Escorial (Brooks *et al.*, 2000) and electrodiagnostic (De Carvalho *et al.*, 2008) criteria and confirmed by neuropathological examination in accordance with published guidelines (Piao *et al.*, 2003).

The patient study protocol was approved by the institutional clinical study committee at Tokyo Medical and Dental University (No. 799). Consent forms for autopsy were obtained from legal representatives of all patients in accordance with the guidelines of the institutional review boards.

Animals

Ten male adult cynomolgus monkeys (*Macaca fascicularis*; 3–7 years old, 3.28–5.10 kg) were bred and treated at Tsukuba Primate Research Centre. The number of monkeys and concentrations of viral stocks were as follows: one monkey was injected with high-dose Flag-TDP-43 AAV1 [1×10^{13} viral genomes (vg)/ml]; six monkeys were injected with low-dose Flag-TDP-43 AAV1 (3×10^{12} vg/ml); three monkeys were injected with low-dose mock AAV1 (3×10^{12} vg/ml) as a negative control. Three monkeys injected with low-dose TDP-43 AAV1 were pathologically examined in the early stage, 3–5 days after the onset of motor symptoms and the other three monkeys were examined in the late stage, 4–7 weeks after injection.

Eleven adult male Fisher rats (10 weeks old, Sankyo-lab) were used. The number of rats and concentrations of viral stocks were as follows: eight rats were injected with low-dose Flag-TDP-43 AAV1 (3×10^{12} vg/ml) and three rats were injected with low-dose control AAV1 (3×10^{12} vg/ml) as a negative control. Three rats injected with TDP-43 AAV1 were pathologically examined in the early stage, 1–2 weeks after injection, and the others were examined in the late stage, 4–9 weeks after injection.

All animal experiments were conducted according to the U.S. National Institutes of Health Guide for the Care and Use of Laboratory Animals, and the Guidelines for the Animal Care and Management of the Tsukuba Primate Research Center and Tokyo Medical and Dental University.

Constructs

Human wild-type TDP-43 was purchased from Invitrogen. The TDP-43 and Flag-TDP-43 fragments were generated by polymerase chain reaction using the following primer pairs: 5′-CCGCTCGAGGCCACCATG GATTAC AAGGATGACGACGATAAGTCTGAATATATTCGGGTAA CCGG-3′ and 5′-CCGCTCGAGCTACATTCCCCAG CCAGAAG ACTTA-3′ for TDP-43, and 5′-CCGCTCGAGGCCACCATGGATTACA AGGATGACGACGAT AAGTCTGAATATATTCGGGTAACCGG-3′ and 5′-CCGCTCGAGCTACATTCCCCAGCCAGAAGACTTA-3′ for Flag-TDP-43, which contained XhoI digestion sites at the 3′- and 5′-ends. The Flag-TDP-43 complementary DNA was subcloned into an expression cassette flanked with AAV2 inverted terminal repeats (Stratagene). The cytomegalovirus (CMV) promoter was used to drive expression.

Adeno-associated virus preparations

Human embryonic kidney (HEK) 293 cells at ~70% confluence were transfected with the AAV1 packaging plasmid pRep2/Cap9 (gift from Dr James M. Wilson, University of Pennsylvania) and adenovirus helper plasmid (Stratagene) at a ratio of 1:1:1. At 6 h after transfection, the culture medium was replaced with fresh medium, and the cells were incubated for 48 h. The cells were then harvested from the culture dishes and pelleted by centrifugation, resuspended in phosphate-buffered saline and subjected to three rounds of freeze–thawing. Cell debris was then pelleted by centrifugation at 1200*g* for 15 min. AAV vectors were purified using ammonium sulphate precipitation and iodixanol (Axis-Shield) continuous gradient centrifugation.

Size-exclusion chromatography was performed using an AKTA Explorer 100 HPLC system (GE Healthcare) equipped with a 2-ml sample loop. A Superdex 200 10/300 GL column (GE Healthcare) was equilibrated with MHA buffer (3.3 mM MES, 3.3 mM HEPES, 3.3 mM NaOAc, 50 mM NaCl, pH 6.5). The vector-containing fractions were loaded onto the column at a flow rate of 0.5 ml/min, and the eluate was collected as 0.5 ml fractions over the duration of one column volume (23 ml). AAV peak fractions were identified by 280/260 nm absorbance and real-time quantitative polymerase chain reaction using vector-specific primers. The purified AAVs were then concentrated further by using Amico Ultra-4 tubes (Ultracel-30k, Millipore) to a final concentration of 1×10^{13} genome copies/ml, as determined by real-time quantitative polymerase chain reaction.

The genome copy number was calculated by TaqMan® PCR (Applied Biosystems). The vectors were treated with Benzonase® and digested with proteinase K (Wako Pure Chemical Industries) for 1 h and purified by phenol–chloroform extraction. The TaqMan® primers and probe were designed as follows: forward primer: 5′-CAGGCTGGT CCAACTCCTA-3′, reverse primer: 5′-GCAGTGGTTCACGCCTGTAA-3′, and probe: 5′-TACCCACCTTGGCCTC-3′. The designed TaqMan® PCR fragment was located in the human growth hormone polyadenylation site in the vector.

Successful viral assembly of control AAV and transgene expression were confirmed by immunoblot analysis using HEK 293 cells infected with AAV (Supplementary Fig. 1), as described below.

HEK-293 cells were cultured in Dulbecco's modified Eagle's medium containing 10% foetal bovine serum with 1% penicillin/streptomycin. The cells in 12-well plates were infected by Flag-TDP-43 AAV1 (5×10^{10} vg/ml). At 48 h after infection, cells were harvested by gentle scraping in lysis buffer [20 mM Tris–HCl, 150 mM NaCl, 1% NP-40, 0.1% deoxicolate, 1% sodium dodecyl sulphate, 1 mM EDTA, 1 mM EGTA, 10 mM β-glycerophosphate, 5 mM NaF and Complete protease inhibitor cocktail (Roche Diagnostics)]. Equal amounts of total cellular protein were mixed with 5× Laemmli sample buffer, denatured at 95°C for 5 min, and separated with 10% sodium dodecyl sulphate polyacrylamide gel electrophoresis. The proteins were transferred to PVDF membranes. After blocking with 3% gelatin (Wako Pure Chemical Industry) in Tris-buffered saline or 5% skimmed milk (Wako Pure Chemical Industry) in Tris-buffered saline-Triton X-100, the membranes were incubated overnight with the following primary antibodies: anti-M2 (1:2000); anti-pan-TDP-43 (1:2000); and anti-VP1, VP2 and VP3 of AAV (1:1000). After incubation with an appropriate horseradish peroxidase-conjugated secondary antibody (Santa Cruz Biotechnology), labelling was detected with the ECL Plus™ Chemiluminescent Detection System (GE Healthcare) or SuperSignal (Thermo Scientific).

Stereotaxic injection of adeno-associated viral vectors

All surgical operations were performed under general anaesthesia. Ketamine hydrochloride (Ketalar, Sankyo) was intramuscularly administered at a dose of 5 mg/kg as a pre-anaesthetic agent, and general anaesthesia was maintained with isoflurane (Forane, Abbott) and oxygen after tracheal intubation. The monkeys were positioned in a stereotaxic frame. After a bilateral laminectomy and opening the dura in the midline at C5–6, AAV vectors were stereotaxically injected into the side ipsilateral to the dominant hand. The injection site was determined and depth of needle insertion was calculated from the preoperatively taken MRI of cervical spinal cord. AAV stock (5 μl) was injected through a 31-gauge needle connected to a 10-μl Hamilton microsyringe in 2 min. The needle remained in place for 10 min and was removed slowly. The dura and skin were sutured and monkeys returned to their individual cages. The monkeys received 0.5 mg/kg butorphanol tartrate (Stadol, Bristol-Myers Squibb) intramuscularly for 3 days to alleviate any postoperative pain.

The rats were anaesthetized with an intraperitoneally administered cocktail of 1.5 ml chloral hydrate (70 mg/ml, Wako Pure Chemical Industry) and 0.1 ml ketamine hydrochloride (70 mg/ml) at a dose of 6 ml/kg. A left side hemi-laminectomy was performed from C4 to C6. On the left side of the C6 segment, 1.5 µl of viral stock was manually injected through sharpened microcapillary glass (PN-30 puller, Narishige) connected via silicone to a 10-µl Hamilton microsyringe at a rate of 0.5 µl/min. The sharpened microcapillary glass remained in place for 3 min and was removed slowly. The skin was sutured, the rats placed on a heating pad until they began to recover from surgery, and then returned to their individual cages.

For detection of the AAV genome in the spinal cord, total DNA was extracted from spinal cord with homogenized buffer containing 0.5% sodium dodecyl sulphate, 10 mM Tris–HCl pH 8.0, and 10 mM EDTA pH 8.0, and polymerase chain reactions were carried out with the following primer pair: 5′-CGCTGTTTTGACCTCCATAGAA-3′ and 5′-AGGCGGTACTTACGTCACTCTTG-3′ for the cytomegalovirus β-globin intron.

Behavioural analysis

For monkeys, to evaluate weakness of the forelimb muscles on the AAV-injected side (the dominant-hand side), we performed the 'apple test'. The front fence of the cage was altered to have two holes and trays on the right and left side. A piece of apple was placed in line from back (monkey side) to front (observer side) on the left or right tray at 3, 6, 9 and 12 cm from the front fence during a session. The monkeys were trained to reach a small piece of apple on the trays through the hole. Four sessions were performed alternately for each side. We analysed how frequently a monkey used his dominant hand to pick up apples before and every week after the operations. We also carefully observed behaviour of the monkeys in daily life every day and recorded video monitoring for 30 min per week.

For rats, to evaluate weakness of the forelimb muscles, we measured grip strength using a special device (Muromachi Kiki) as previously described (Anderson, 2005).

Electrophysiological assessment

The nerve conduction study and needle EMG studies were performed under anaesthesia with a combination of 7 mg/kg ketamine hydrochloride and 1.2 mg/kg xylazine administrated intramuscularly. Nerve conduction studies were performed in the bilateral median nerves using conventional procedures and an EMG Machine (MEB-2300, Nihon-koden). The recording surface electrode was placed over the belly of the thenar eminence with a reference electrode at the metacarpophalangeal joint of the thumb, and compound muscle action potentials were elicited after the stimulation of the median nerve at the wrist. The peak-to-peak amplitudes were measured for all compound muscle action potentials. Nerve conduction studies were examined before AAV injection and every 1 or 2 weeks after. The needle EMG study was performed in the first dorsal interosseous, flexor carpi ulnaris and biceps brachii muscles using a conventional concentric needle electrode used in human studies (TECA Elite, CareFusion), 4–6 weeks after AAV injection.

Neuropathological examinations

Animals were deeply anaesthetized first with intramuscularly administered 7 mg/kg ketamine hydrochloride and then with intravenously administered 25 mg/kg pentobarbital. After confirming the absence of a blink reflex, the spinal cord and skeletal muscles were removed. For neuropathological examination, human and animal spinal cord samples were immersion fixed in 10% neutral buffered formalin, processed conventionally, embedded in paraffin, cut into 4-µm-thick sections and stained with haematoxylin and eosin. For immunostaining, sections were deparaffinized, pretreated in 0.5% periodic acid, autoclaved for 5 min at 121°C and then incubated free-floating overnight at 4°C with the following primary antibodies: M2 (1:500), anti-pan-TDP-43 (1:1000), anti-pS409/410-TDP-43 (1:500), anti-ubiquitin (1:500), anti-p62 (1:500), anti-cystatin-C (1:1000), anti-GFAP (1:500), anti-GLUT-5 (1:500) and SMI31 (1:200). Following brief washes, the sections were sequentially incubated with polymer immunocomplex (Dako)

Immunoreactive elements were visualized by treating sections with 3,3′ diaminobenzidine tetroxide (DAB-4HCl, Dojin Kagaku) with or without nickel ammonium chloride. The sections were then counterstained with haematoxylin. For double-immunostaining, the deparaffinized sections were stained with Sudan Black B to avoid autofluorescence. The free-floating sections were incubated overnight at 4°C in solutions containing the primary antibodies. The sections were then incubated with AlexaFluor 488- or 555-conjugated secondary antibodies (1:500, Invitrogen), and DAPI nuclear stain (1:500, Santa Cruz Biotechnology) for 1 h. All sections were examined using a confocal microscope (NIKON or Carl Zeiss).

Animal anterior root samples were fixed with a mixture of 2.5% glutaraldehyde in 0.1 M phosphate buffer (pH 7.4) at 4°C overnight, and then further fixed in 1% osmium tetroxide in 0.1 M phosphate buffer (pH 7.4) for 1 h. The well-fixed tissues were dehydrated in graded ethanol and embedded in Epon 812 (Poly/Bed® 812, Polyscience). The fixed roots were transversely cut into 1-µm-thick sections and stained with toluidine blue.

For counting of anterior horn neurons in the spinal cord, monkey eighth cervical segments were serially cut at 4-µm thickness, and every fifth section was stained with haematoxylin and eosin. The previous and next serial sections (that is, every fourth and sixth sections) were immunostained with anti-pan-TDP-43 or anti-Flag antibodies. The number and minimum diameters of neurons with nuclei in the lateral or medial nuclear groups in 15 sections were evaluated using the Image J software program from the U.S. National Institutes of Health.

Antibody information

We used the following primary antibodies for immunostaining and immunoblot analyses: mouse monoclonal anti-Flag (M2, Sigma); rabbit polyclonal anti-pan-TDP-43 (10782-1-AP, ProteinTech Group); rabbit polyclonal anti-C-terminal TDP-43 (12892-1-AP, ProteinTech Group); rabbit polyclonal anti-phosphorylated S409/410 TDP-43 (Cosmo Bio); rabbit polyclonal anti-ubiquitin (Dako); rabbit polyclonal anti-cystatin-C (Dako); mouse monoclonal anti-phosphorylated neurofilament (SMI31, Sternberger Monoclonals); rabbit polyclonal anti-glial fibrillary acidic protein (GFAP) (Dako); rabbit polyclonal anti-glucose transporter 5 (GLUT-5, IBL); rabbit polyclonal and mouse monoclonal anti-peripeherin (AB1530 and AB1527, Chemicon); mouse monoclonal anti-neurofilament light (N5139, Sigma) antibody; anti-p62 (GP62-C, Progen); anti-glyceraldehyde-3-phosphate dehydrogenase (GAPDH, Biodesign), and anti-AAV capsid proteins VP1, VP2 and VP3 (Progen Biotechnik).

Sequential biochemical fractionation, dephosphorylation and immunoblot analysis

Frozen frontal cortex or spinal cord (50–250 mg) was homogenized in 10 volumes of buffer A (10 mM Tris–HCl pH 7.5, containing 1 mM

EGTA, 10% sucrose and 0.8 M NaCl). After the addition of Triton X-100 at a final concentration of 1%, the homogenate was incubated for 30 min at 37°C and spun at 100 000*g* for 20 min at 20°C. The pellet was homogenized in 20 volumes of buffer A containing 1% sarkosyl, incubated for 30 min at 37°C and spun at 100 000 *g* for 20 min at 20°C. The sarkosyl-insoluble pellet was homogenized in four volumes of buffer A containing 1% CHAPS [3-[(3-cholamidopropyl)dimethylammonio]-1-propanesulphonate] and spun at 100 000*g* for 20 min. The pellet was sonicated in 0.5 volume of 8 mol/l urea buffer, cleared by centrifugation at 100 000*g* for 20 min at 20°C, and used for immunoblotting. The samples before (−) and after (+) treatment with lambda protein phosphatase (1600 U/ml, New England Biolabs) were subjected to 10% sodium dodecyl sulphate polyacrylamide gel electrophoresis. Proteins in the gel were then transferred onto a polyvinylidene difluoride (PVDF) membrane (Millipore). After blocking with 3% gelatin (Wako Pure Chemical Industries) in Tris-buffered saline (50 mM Tris–HCl pH 7.5, 150 mM NaCl), the membranes were incubated overnight with the following primary antibodies: anti-M2 (1:2000); anti-C-TDP-43 (1:1200); anti-phosphorylated S409/410 TDP-43 (1:2000); anti-p62 (1:3000) and anti-GAPDH (1:2000). After incubation with an appropriate horseradish peroxidase-conjugated secondary antibody (Santa Cruz Biotechnology), labelling was detected by a 3,3′diaminobendizene reaction intensified with nickel chloride (Metal-Enhanced DAB Substrate Kit, Thermo Scientific), the ECL Plus™ Chemiluminescent Detection System (GE Healthcare), or SuperSignal (Thermo Scientific).

Quantitative real-time polymerase chain reaction assay

Total RNA was extracted from whole-brain homogenates with Isogen (Nippon Gene). DNase-treated RNA (2.5 μg) was reverse-transcribed with SuperScript® III and random hexamers (Life Technologies). Complementary DNA was amplified by the quantitative TaqMan® system by using the Light Cycler 480 Real-Time PCR Instrument (Roche Diagnostics). The primers and probes specific for Flag-tagged human TDP-43, rat TDP-43 (NM_001011979.2) and monkey TDP-43 (XM_001102660.2) were designed. Relative Flag-human TDP-43 messenger RNA levels were calculated in comparison to endogenous rat or cynomolgus messenger RNA levels. A list of all primers and probes used in this study is provided in Supplementary Table 1.

Statistical analysis

The data obtained from independent experiments are presented as means ± SEM.

Statistical analysis of spinal neuron counts and axonal density among TDP-43-expressed monkey group in early, late stage and control monkey group by one-way ANOVA with Bonferroni's *post hoc* test. $P < 0.05$ was considered significant.

Results

Overexpressing wild-type TDP-43 in the monkey cervical cord leads to progressive motor weakness and muscle atrophy with fasciculation

AAV expressing Flag-tagged TDP-43 (Supplementary Fig. 2) was directly injected into the sixth cervical segment on the dominant-hand side of seven monkeys. All monkeys developed progressive motor weakness and muscle atrophy with marked fasciculation in the forelimb on the injected side (Fig. 1A and B, Supplementary Video 1). Two to 3 weeks after the injection, the TDP-43-expressing monkeys first showed some difficulty in taking time to pick up pieces of apple using the dominant hand on the injected side in the apple test, and changed to use the non-dominant hand (Fig. 1C). On observation by video monitoring, they could reach and grasp the ceiling fence at the onset of clumsiness of picking apples, but 1–3 weeks later could not flex the elbow joint and raise the forelimb, indicating the motor weakness had spread to the proximal muscles (Fig. 1D). In the late stage, 2–5 weeks after the onset, the dominant hand muscles became completely paralysed (Fig. 1A), and muscle weakness and atrophy had spread to the contralateral, un-injected side limb muscles (Fig. 1B and E). One of TDP-43-expressing monkeys showed respiratory failure at the end stage. The control monkeys did not show obvious motor symptoms, indicating surgical procedure or virus toxicity was minimal (Fig. 1C–E and Supplementary Video 2).

Electrophysiological findings

Electrophysiologically, in all TDP-43-expressing monkeys, the compound muscle action potential of the thenar muscle evoked by stimulation of the median nerve at the wrist progressively decreased in size with preservation of conduction velocity, and the muscle became unexcitable in the late stage (Fig. 2A). In contrast, three monkeys injected with control AAV did not show a marked change compound muscle action potential size (Fig. 2A). In TDP-43-expressing monkeys, the compound muscle action potential size on the contralateral side was not changed in the early stage (3–5 days after the onset of motor symptoms), but showed milder reduction of compound muscle action potential size in the late stage (Fig. 2B). Needle EMG revealed robust fasciculation potentials, and denervating potentials of positive sharp waves and fibrillation potentials in the late stage (Fig. 2C).

Cytoplasmic mislocalization with loss of endogenous monkey TDP-43, dystrophic neurites and cystatin C-positive granules in the cytoplasm

Neuropathologically, an anti-Flag antibody widely detected exogenous TDP-43 in neurons from the second cervical to the second thoracic segments on both sides, and was observed in almost all neurons on the injected side from the fourth to eighth cervical segments. Generally, Flag immunoreactivity was not detected in the glial cells. There was no inflammatory reaction except for in the area around the injection site. In the late stage, exogenous TDP-43 was observed in either the nucleus or cytoplasm (Fig. 3A). Pan-TDP-43 staining revealed that most motoneurons with cytoplasmic TDP-43 lost endogenous monkey TDP-43 staining (Fig. 3B), which normally localized in the nucleus (Fig. 3C). Mislocalized TDP-43 was diffusely distributed in the cytoplasm

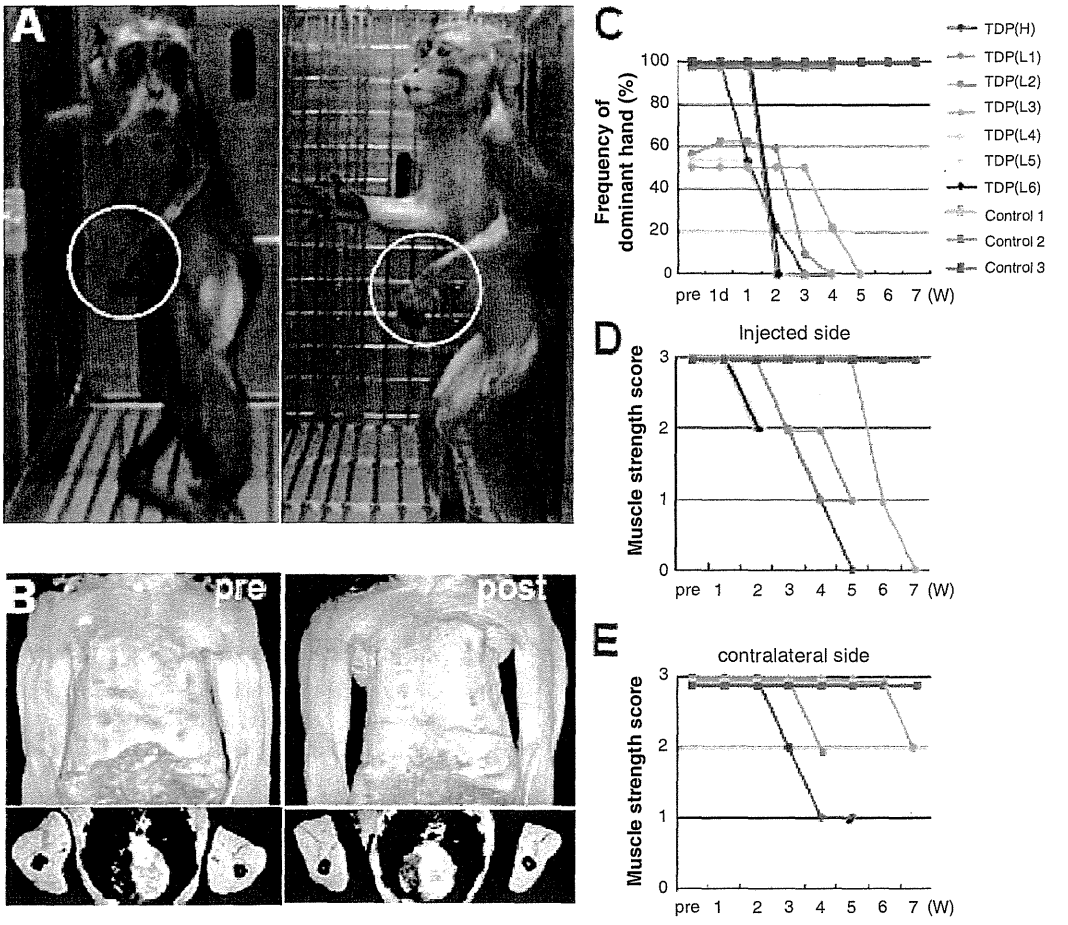

Figure 1 Overexpressing wild-type TDP-43 in the monkey cervical cord leads to progressive motor weakness and muscle atrophy. (**A**) Motor paresis of the forelimb on the injected side (encircled) in TDP-43 AAV-injected monkeys. (**B**) Constructed (*top*) and axial (*bottom*) MRI images of upper arm muscles before (pre) and 4 weeks after (post) injection, indicating a marked muscle atrophy of upper and forearms as well as hand muscles, predominantly on the injected side (left side). (**C**) Apple test. Frequency with which the dominant hand was used to pick up apples. (**D** and **E**) Behavioural analysis assessing muscle strength of forearms on the injected side (**D**) and contralateral side (**E**). A score of 3 indicates that the monkeys can hang on the ceiling fence; score of 2, they can grasp but not hang on the ceiling fence; score of 1, they can raise the forelimb but not reach ceiling fence; score of 0, they cannot raise the forelimb. Measurements that appear to end before the end of the experiment are from the three monkeys that were pathologically examined in the early stage.

and, in some neurons, granularly aggregated (Fig. 3B). Proximal and distal dystrophic neurites were occasionally observed (Fig. 3A and B). Phosphorylation of TDP-43 in the nucleus or cytoplasm was not clear in the early stage, but became obvious in the late stage (Fig. 3D). Anti-ubiquitin and anti-p62 antibodies did not show a clear abnormal signal. Astrogliosis and microgliosis were observed (Supplementary Fig. 3). A small fraction of the motoneurons expressing TDP-43 in the nucleus characteristically displayed coarse cystatin C-positive granules in the cytoplasm (Fig. 3E) in the neurons with exogenously expressed TDP-43 in the nucleus. There were no neurons with co-localized cystatin C-positive granules and TDP-43 aggregates in the cytoplasm. We also observed aberrant accumulation of phosphorylated neurofilaments (Fig. 3F) and peripherin (Supplementary Fig. 4) in the cytoplasm of spinal motoneurons, a common pathological feature in patients with ALS (Munoz *et al.*, 1988; Corbo and Hays, 1992). Immunostaining with an anti-Flag antibody identified its nuclear or cytoplasmic immunoreactivity in some Betz cells in the precentral gyrus restricted to the forelimb area contralateral to the injection. This Flag immunoreactivity was not observed in other cortical areas (including hippocampus and frontal lobe, which are preferentially affected in patients with FTLD), thalamus, basal ganglia and white matter, or in glial cells (Supplementary Fig. 5).

Characteristic regional mislocalization of TDP-43 in motoneurons of the anterior horn similar to amyotrophic lateral sclerosis spinal cords

In the early stage, 3–5 days after the onset of hand clumsiness, TDP-43 mislocalization of diffuse staining pattern was observed in

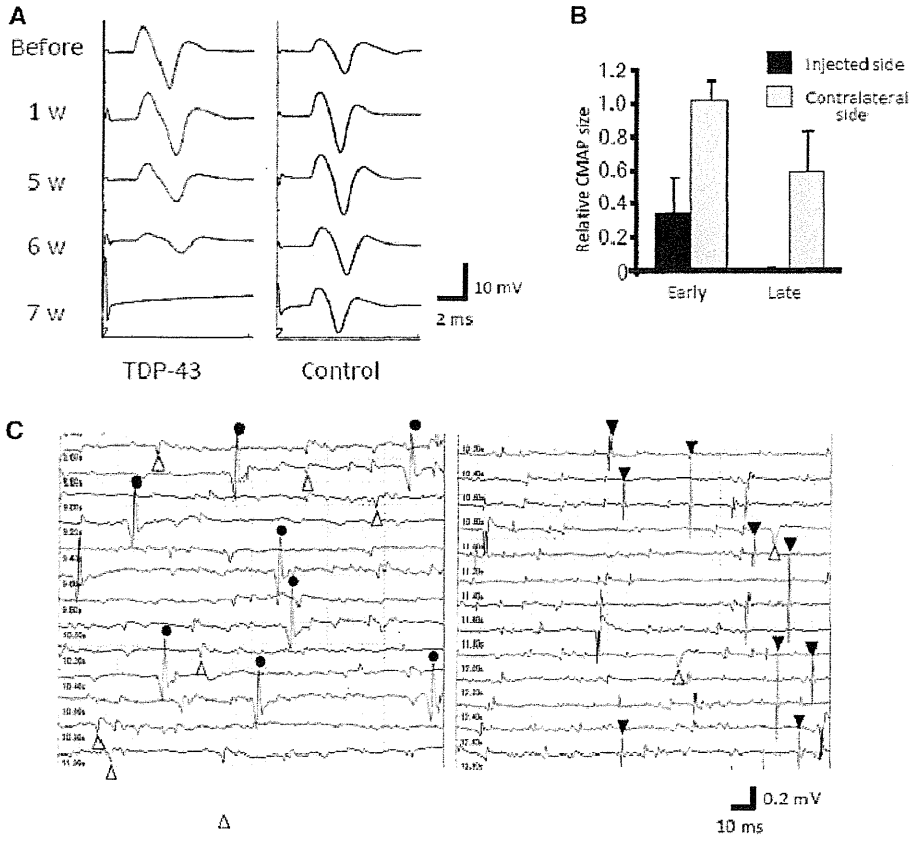

Figure 2 Electrophysiological findings for motor symptoms of the monkeys. (**A**) Compound muscle action potentials (CMAPs) in the thenar muscle after stimulation of the median nerve at the wrist. They gradually decreased in size, and became inexcitable in the late stage. There was no change of compound muscle action potential size in the control monkey. (**B**) Ratio of the compound muscle action potential size 3–5 days after the onset (early stage) or 2–5 weeks after the onset (late stage) to the size before injection. In the early stage, there was no reduction in compound muscle action potential size on the contralateral side, but moderately attenuated in the late stage. (**C**) Needle EMG findings of the forearm muscle. Circles indicate fasciculation potentials; open triangles, positive sharp waves; filled triangles, fibrillation potentials.

most motoneurons in the lateral nuclear group of the anterior horn. In contrast, almost all neurons in other areas of the spinal cord including the posterior horn showed flag signal of exogenously expressed TDP-43 only in the nucleus (Fig. 4A and D). Importantly, the contralateral lateral nuclear group also exhibited TDP-43 mislocalization on the side of forelimb that did not yet show obvious motor symptoms (Supplementary Fig. 6). Signals of exogenous Flag-TDP-43 were detected by real-time polymerase chain reaction on the contralateral half of the spinal cord (Supplementary Fig. 7). However, this distribution indicates that this regional selectivity is not due to differences in the concentration of the injected AAV, but rather is due to properties of the affected neurons. In the late stage, 2–5 weeks after onset, the percentage of motoneurons with TDP-43 mislocalization decreased ~47% in the lateral nuclear group, and was <2% in the ventromedial nuclear group (Figs 3B and 4D). The number of large motoneurons ($\geqslant$20 μm) in the early stage in this lateral nuclear group did not change, but in the late stage, was reduced by ~42% (Fig. 4B, C and E). In contrast, the reduction in the number of large neurons in the ventromedial nuclear group was not significant (control, 1.78 ± 0.20 versus TDP-43, 1.68 ± 0.18/section, $P = 0.80$). Astrogliosis was also more prominent in the lateral area than in the ventromedial area of the anterior horn (data not shown). Motoneuronal degeneration of the lateral nuclear group was also confirmed by studying the anterior roots of the eighth cervical segment, which showed frequent myelin ovoids and loss of large myelinated axons ($\geqslant$8 μm) in the late stage, although they were almost normal in the early stage (Fig. 5A–C). This axonal loss in the anterior roots is consistent with pathological change of the thenar muscle, showing numerous small angulated atrophic fibres (Fig. 5D).

We furthermore examined whether such a regional change of TDP-43 mislocalization occurs in spinal cord of nine patients with ALS with upper limb weakness and hand muscle atrophy. TDP-43 mislocalization was observed much more in the lateral nuclear group than in the ventromedial nuclear group of the cord at the eighth cervical segment (Fig. 6A–C).

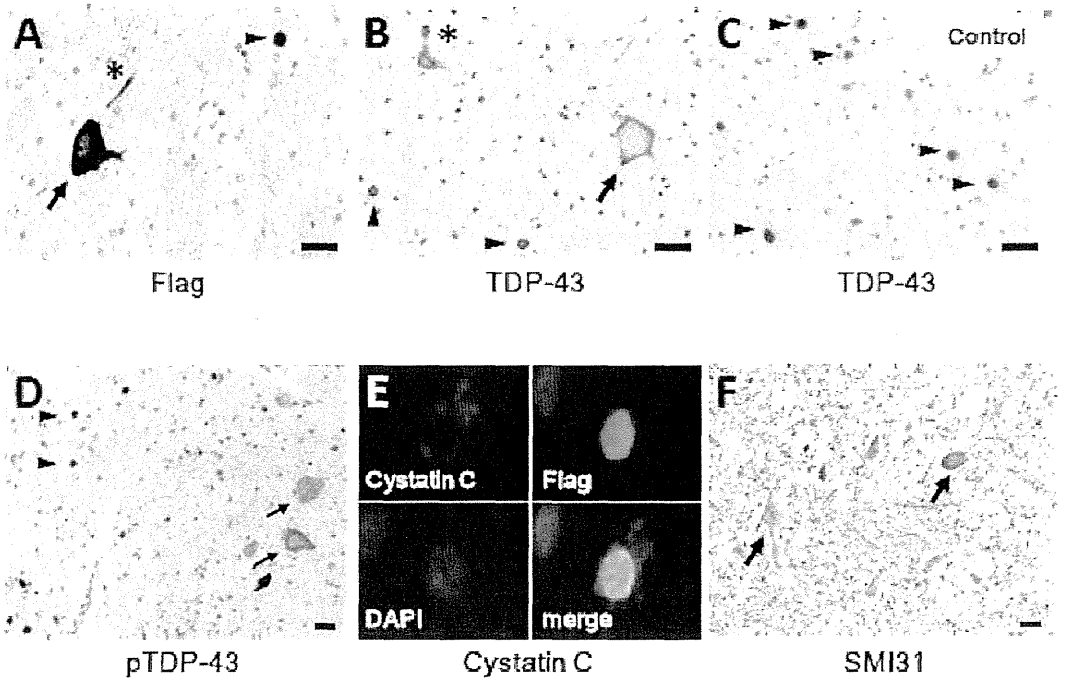

Figure 3 Neuropathological findings of monkey spinal cords of TDP-43–overexpressed monkeys at the late stage (**A**, **D–F**), and control with mock AAV (**C**). (**A–D**) TDP-43-overexpressed spinal cord immunostaining using antibodies to Flag (**A**), pan-TDP-43 (**B**) and pS409/410 TDP-43 (**D**) demonstrated mislocalization in cytoplasm (arrows), and dystrophic neurites (asterisks) as well as normal localization in nuclei (arrowheads), whereas normal spinal cord showed only nuclear localization of TDP-43. (**E**) Co-labelling of a motoneuron expressing TDP-43 in the nucleus with antibodies to cystatin C (red) and Flag (green). The nucleus is labelled with DAPI. (**F**) Immunostaining using SMI31 revealed the aberrant presence of phosphorylated neurofilament in the neuronal cytoplasm (arrows). Scale bars: 20 μm. Immunostainings of spinal cord with control mock AAV using the antibodies to Flag, pS409/410 TDP-43, cystatin C and SMI31 are shown in Supplementary Fig. 7.

Interspecies differences in TDP-43 pathology in rodents and primates

To investigate interspecies differences in TDP-43 pathology, we injected the identical TDP-43-expressing AAV at the same concentration into rat cervical cords. Expression level of Flag-TDP-43 messenger RNA around the injection site in rat spinal cord was >20-fold higher than that of endogenous TDP-43 level, and this fold change was similar to that in monkey spinal cord (Fig. 7A). Rats injected with TDP-43 AAV showed progressive motor weakness (Fig. 7B), measured by grip strength. Importantly, exogenous TDP-43 was observed only in the nuclei of motoneurons in both early (14 days after injection of AAV) and late (4 weeks after injection of AAV) stages (Fig. 7C). Since mislocalization of TDP-43 in the monkey spinal cords was more prominent in the early stage (14 days), we also examined the pathology of rat spinal cords at a very early stage (7 days); however, the weak Flag immunoreactivity was still limited to the nucleus of motoneurons (data not shown). Furthermore, this rat model failed to exhibit cystatin C-positive aggregates, dystrophic neurites, or aberrant accumulation of phosphorylated neurofilaments in the cytoplasm of spinal motoneurons (Fig. 7D). These neuropathological findings indicate that this rat model was less similar to human ALS than our monkey model in TDP-43 localization and other characteristic features of ALS.

Detection of the 25-kDa C-terminal fragment and phosphorylated TDP-43 in the early stage

Biochemically, immunoblot analysis of monkey spinal cord demonstrated that the exogenous Flag-tagged TDP-43 became much more insoluble than endogenous TDP-43 (Fig. 8A). The phosphorylation of TDP-43 was unclear in the early stage (Fig. 8B) but clearly detected later (Fig. 8C). Neither a C-terminal nor a phosphospecific TDP-43 antibody detected the 25-kDa C-terminal fragment (Fig. 8A–C). These suggest that neither phosphorylation of TDP-43 or its 25-kDa C-terminal fragment in spinal cord is necessary to initiate motoneuronal dysfunction and degeneration in our monkeys.

Discussion

Frequent mislocalization of TDP-43 in the cytoplasm and loss of its nuclear staining are major pathological hallmarks in the histological

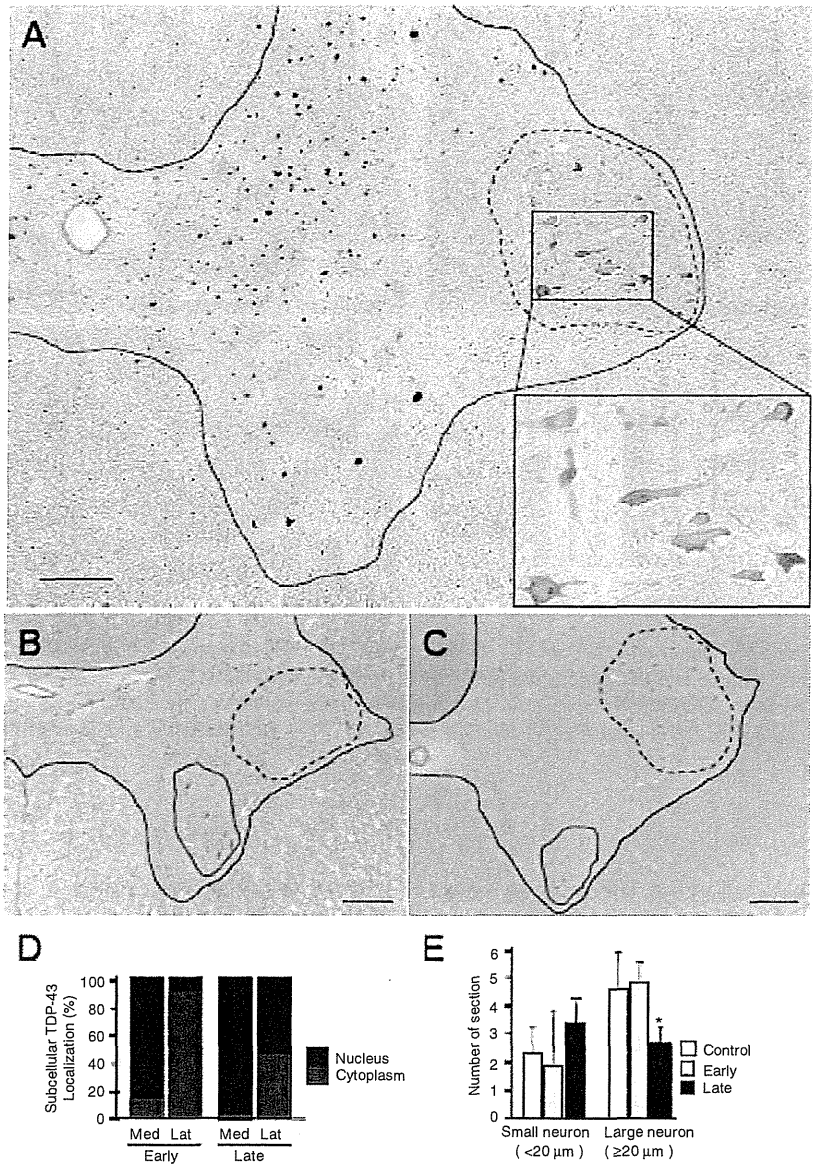

Figure 4 Regional mislocalization of TDP-43 and cell death in monkey spinal cords. (**A**) Sections from the injected side of the eighth cervical segment of the cord taken at the early stage and immunostained with an anti-Flag antibody. Most neurons in the lateral nuclear group (area encircled by broken line) showed cytoplasmic mislocalization of TDP-43 (inset), but almost all neurons in other areas expressed exogenous TDP-43 in the nucleus. Scale bars: 200 μm. (**B** and **C**) The eighth cervical level of cord from monkeys injected with TDP-43–expressing (**B**) and control (**C**) AAV, taken at the late stage and stained with haematoxylin and eosin. The number of large motoneurons decreased in the lateral nuclear group (areas encircled by broken line), but not in ventromedial nuclear group (areas encircled by red solid line). Scale bars: 200 μm. (**D**) Percentage of neurons with nuclear (black) or cytoplasmic (red) localization of exogenous TDP-43 in the lateral nuclear groups on the injected side. Neurodegeneration affects the lateral nuclear group more than the ventromedial nuclear group. (**E**) Cell count of neurons in the lateral nuclear group on haematoxylin and eosin staining. Mean ± SEM. $n = 3$, $^*P < 0.05$. Lat = lateral nuclear group; Med = ventromedial nuclear group.

diagnosis of ALS and FTLD (Geser *et al.*, 2010). The classification of TDP-43 proteinopathy is based on a combination of neuronal cytoplasmic inclusions and dystrophic neurites (Mackenzie *et al.*, 2011). The morphological features in our monkeys are close to type B TDP-43 proteinopathy, which is usually observed in the brains of patients with ALS. The only difference between the pathology of our monkeys and type B TDP-43 proteinopathy is that mislocalized cytoplasmic TDP-43 was usually diffuse and neuronal cytoplasmic inclusions were less frequent in our monkeys. Since this monkey is an acute model for TDP-43 pathology, it possibly

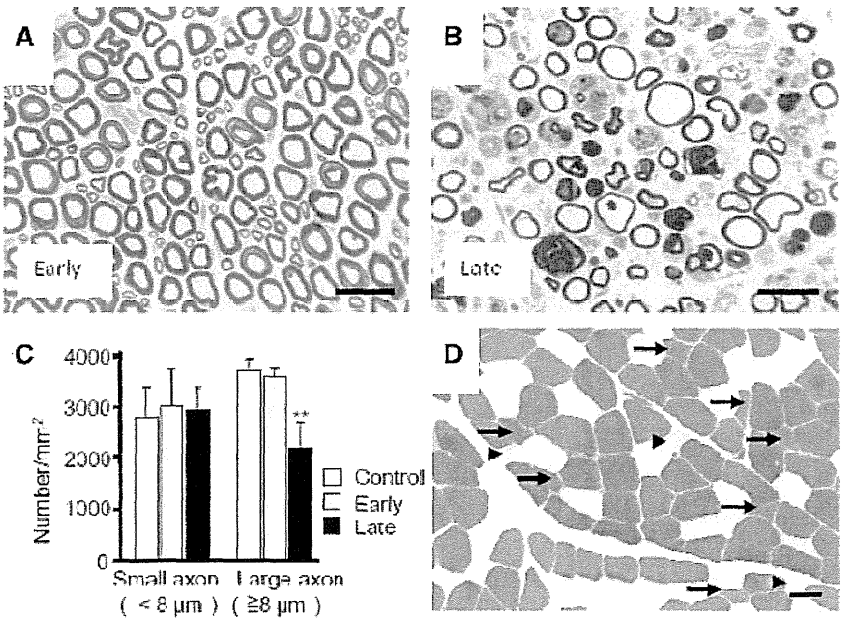

Figure 5 Pathological finding of monkey anterior root and skeletal muscle. Toluidine blue staining of the eighth cervical anterior roots on the injected side in the early (**A**) and late (**B**) stages, and their myelinated axon densities (**C**). Mean ± SEM, $n = 3$, $^{**}P < 0.01$. (**D**) Transverse section of the biceps brachii muscle from a TDP-43–expressing monkey 4 weeks after injection, stained with ATPase (pH 10.6). Small angulated atrophic changes of type I (arrowheads) and type II (arrows) fibres, with predominant involvement of type II fibres, can be seen. Scale bar: 50 μm.

takes more time for diffusely mislocalized TDP-43 to be aggregated. Moreover, in the spinal cords of patients with ALS, diffuse cytoplasmic TDP-43 staining is more common, and neuronal cytoplasmic inclusions are less frequent than in the brain and may even be absent (Giordana *et al.*, 2010). Thus, our monkey model shows the key features of TDP-43 proteinopathy as seen in the ALS spinal cord.

Interestingly, despite the diffuse expression of exogenous TDP-43 in the spinal cord, TDP-43 mislocalization and neuron loss predominantly occurred in the lateral nuclear group in Rexed lamina IX, in which large neurons are mostly α-motoneurons (Carpenter *et al.*, 1983). The sensory neurons and interneurons in laminae III–VIII rarely showed TDP-43 mislocalization, and large motoneurons in the ventromedial nuclear group, most of which are also α-motoneurons, showed much less TDP-43 mislocalization and neuron loss. Within lamina IX, the lateral nuclear group innervates the distal, fast-contracting muscles of the extremities, and the ventromedial nuclear group innervates the posture-related, continuously contracting muscles attached to the axial skeleton (Carpenter *et al.*, 1983). This regional vulnerability among α-motoneurons is consistent with the distal hand or foot muscles being the first involved in 73% of patients with non-bulbar ALS (Harverkamp *et al.*, 1995; Körner *et al.*, 2011) and might be related to axon length, which affects axonal transport (Bilsland *et al.*, 2010), or to the preferential susceptibility of fast-fatigue rather than slow motoneurons (Dengler *et al.*, 1990; Pun *et al.*, 2006). Furthermore, in nine patients with ALS, more TDP-43 mislocalization was observed in the lateral nuclear group than in the ventromedial nuclear group of the eighth cervical cord segments. Taking these results together, we think that the tropism of TDP-43 mislocalization was similar to that of ALS pathology. However, expression levels of exogenous wild-type TDP-43 in our monkey and rat models were very high (~20-fold higher than that of endogenous TDP-43), which was partly due to lack of 3′-untranslated region in our TDP-43 expression construct. This is probably because TDP-43 controls its own expression through a negative feedback loop by binding to 3′-untranslated region sequences in its own messenger RNA (Ayala *et al.*, 2010; Polymenidou *et al.*, 2010). The unphysiologically high level of TDP-43 expression in our animal models should be taken into consideration when interpreting our findings.

Since Flag TDP-43 messenger RNA was detected in the spinal cord contralateral to the injected side by real-time polymerase chain reaction analysis, the AAV virus was shown to spread contralaterally through the spinal cord causing motor paresis and reduction of compound muscle action potential size in the opposite forelimb. However, it is still possible that there was concomitant cell-to-cell or trans-synaptic propagation of Flag TDP-43 protein in the spinal cord. Moreover, it is interesting that the Flag-TDP-43 signal was selectively extended into Betz cells in the forelimb area of precentral gyrus contralateral to the injection side, which can be explained by a retrograde progression from α-motoneuron in the cervical cord. More sophisticated experimental paradigms are necessary to distinguish whether it is the AAV vector itself,

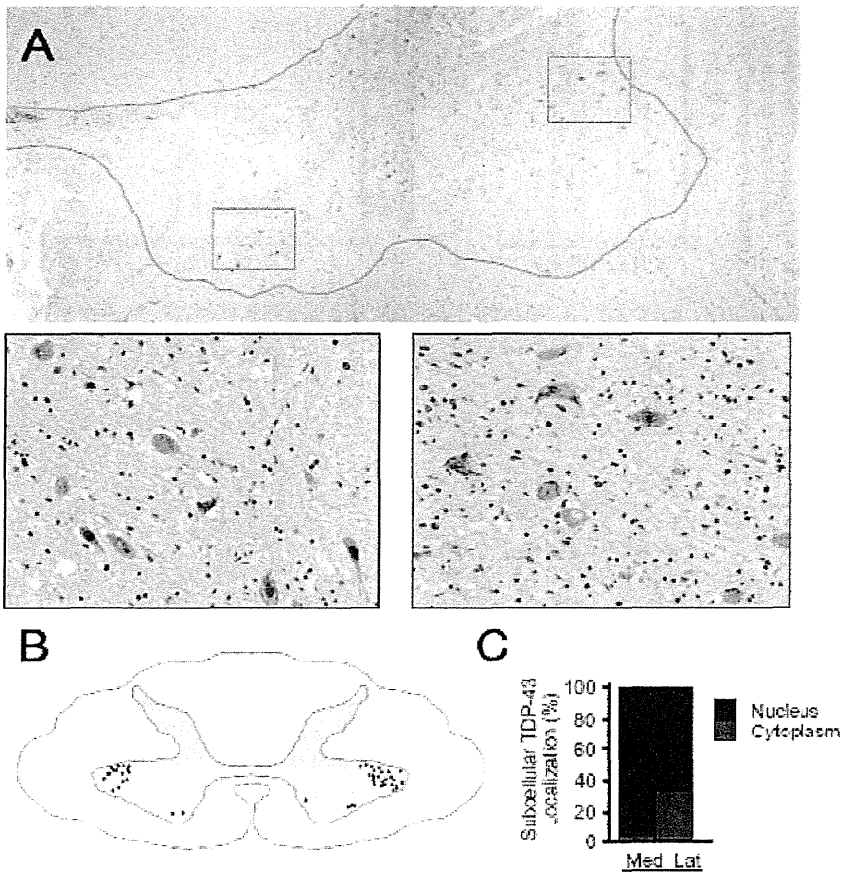

Figure 6 Pan-TDP-43 staining of spinal cords of patients with ALS. (**A**) Autopsied eighth cervical segment of spinal cord immunostained with pan-TDP-43 antibody. Scale bars: 200 μm in **A** and 50 μm in window insets. (**B**) Schematic illustration of the distribution of neurons with TDP-43 mislocalization, made by summing data from five sections (at 20-μm intervals). (**C**) Percentage of neurons with nuclear or cytoplasmic localization of exogenous TDP-43 in the lateral and medial nuclear groups. More frequent TDP-43 mislocalization in the lateral nuclear group in spinal cords of patients with ALS than in the medial nuclear group. Mean ± SEM, $n = 10$, $P < 0.01$. Scale bars: 50 μm. Lat = lateral nuclear group; Med = ventromedial nuclear group.

transcribed messenger RNA or Flag-TDP protein that is the molecule responsible for this progression, which is a prime objective for our future study.

Bunina bodies are small, cystatin C-positive, eosinophilic cytoplasmic inclusions and are generally considered a specific hallmark of sporadic ALS (Okamoto *et al.*, 1993; Mitsumoto *et al.*, 1998). Importantly, Bunina bodies are absent in familial ALS that is due to the SOD1 mutation (Tan *et al.*, 2007) or FUS/TLS mutation (Tateishi *et al.*, 2010), but they have been detected in familial ALS with the TDP-43 mutation (Yokoseki *et al.*, 2008) as well as in sporadic ALS. These imply an association between Bunina bodies and TDP-43 pathology in sporadic ALS. From this point of view, the generation of cystatin C-positive cytoplasmic aggregates in our monkeys might strengthen their pathological value as a model of sporadic ALS.

Biochemically, TDP-43 proteinopathy is characterized by decreased solubility, phosphorylation and the generation of 25-kDa C-terminal fragment (Arai *et al.*, 2006; Neumann *et al.*, 2006; Hasegawa *et al.*, 2008). In TDP-43-overexpressing monkeys, the exogenous TDP-43 became much more insoluble than endogenous TDP-43 of control monkeys, indicating that expression of large amounts of exogenous wild-type TDP-43 can render it insoluble. Unexpectedly, the solubility of endogenous monkey TDP-43 did not become insoluble in TDP-43-overexpressing monkeys. The expectation would be that exogenous insoluble TDP-43 would recruit endogenous monkey TDP-43 and alter its solubility. In this biochemical aspect of TDP-43 solubility, our monkey model differs from patients with ALS.

The pathological role of phosphorylated TDP-43 is still unclear; TDP-43 phosphorylation in culture cells enhances its oligomerization (Hasegawa *et al.*, 2008), but experiments with a phosphorylation-resistant mutant TDP-43 indicated that phosphorylation is not required for inclusion formation or cellular toxicity (Zhang *et al.*, 2009). In our monkeys, phosphorylation of TDP-43 was a late event but not observed at 4 days after symptom onset. This finding suggests that TDP-43 phosphorylation is not

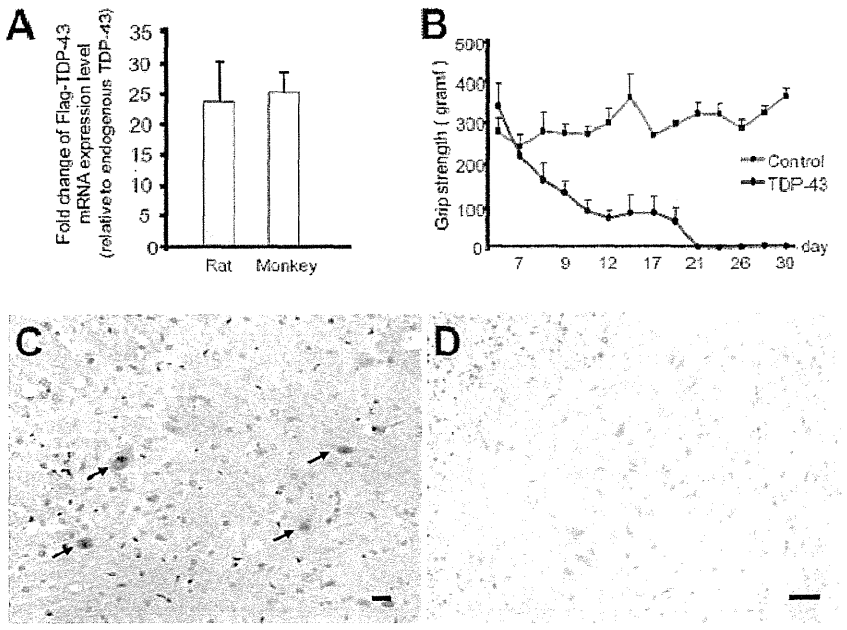

Figure 7 Effect of TDP-43-expressing AAV in rat spinal cords. (**A**) Ratio of exogenously expressed Flag-TDP-43 messenger RNA level to endogenous rat or cynomolgus TDP-43 messenger RNA level evaluated by quantitative real-time polymerase chain reaction. Mean ± SEM, rat, $n = 4$; cynomolgus, $n = 3$, $P = 0.74$. (**B**) Time course of grip strength. Mean ± SEM. (**C**) Nuclear staining of exogenous TDP-43 in cervical cord sections of AAV-injected rats by immunostaining with an anti-Flag antibody (arrows). (**D**) Immunostaining of cervical cord sections of TDP-43–expressing rat, 4 weeks after injection, with SMI31 did not show aberrant phosphorylated neurofilament in the neuronal cytoplasm. Scale bars: 20 μm.

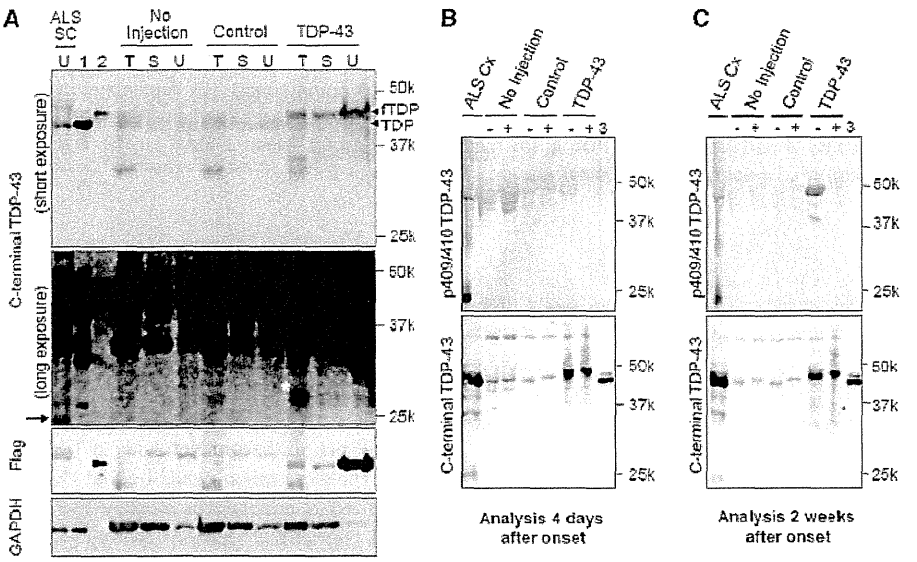

Figure 8 Biochemical analysis of monkey spinal cords. (**A**) Immunoblot of cervical spinal cord lysates from TDP-43–expressing monkeys (4 weeks after injection) and patients with ALS using antibodies recognizing the C-terminus of TDP-43 and Flag. SC = spinal cord of patient with ALS; 1 = TDP-43–expressing HEK 293 T cell lysate; 2 = Flag-TDP-43–expressing HEK 293T cell lysate; T = 1% Triton X-100-soluble; S = 1% sarkosyl-soluble; U = 8 mol/l urea-soluble fraction; fTDP = Flag-TDP-43. A longer exposure (second panel from *top*) revealed the 25-kDa C-terminal fragment in the spinal cord of a patient with ALS (arrow). The ~30-kDa band noted in the Triton-soluble fraction from the spinal cord of a TDP-43–expressing monkey (asterisk) was different from the 25-kDa C-terminal fragment (arrow). (**B** and **C**) Immunoblot of 8 mol/l urea-soluble fraction from the monkey spinal cord harvested 4 days (**B**) and 2 weeks (**C**) after onset of symptoms, using antibodies to pS409/410 TDP-43 (*top*) and C-TDP-43 (*bottom*) before (−) and after (+) treatment with lambda protein phosphatase (λPPase). 3 = Mixture of Flag-TDP-43- and TDP-43-expressing HEK 293T cell lysates. The phosphorylated TDP-43 was detected only in the late stage (asterisk).

necessary to initiate motor symptoms and is a late event in motoneuron degeneration.

In the spinal cords of our monkeys, neither a C-terminal nor a phosphospecific TDP-43 antibody detected the 25-kDa C-terminal fragment that is found in patients with ALS. Overexpressed 25-kDa C-terminal fragment in cultured cells is reported to be toxic (Igaz *et al.*, 2009; Zhang *et al.*, 2009), and the accumulation of 25-kDa C-terminal fragment in transgenic mouse brain correlates with disease progression (Xu *et al.*, 2010). Interestingly, unlike the FTLD/ALS brain, the 25-kDa C-terminal fragment is often absent in the ALS spinal cord (Neumann *et al.*, 2009). The absence of 25-kDa C-terminal fragment in ALS spinal cord does not necessarily preclude a primary role for this form; rather it can be pathologically crucial if its absence is due to the accelerated degeneration of motoneurons with 25-kDa C-terminal fragment. It is difficult to deny that small amounts of C-terminal truncated species are actually present, because mislocalization of TDP-43 was focal in the spinal cord of our monkeys. However, the failure to detect 25-kDa C-terminal fragment in our monkey spinal cord at the early stage may have an implication that full-length TDP-43 is sufficient to be toxic, because α-motor axonal excitability was impaired but their cell bodies were preserved at autopsy.

The results of studies on the relationship between TDP-43 mislocalization and neuron loss remain controversial. The overexpression of wild-type TDP-43 in the nuclei in a transgenic rodent model was sufficient to be toxic to spinal motoneurons (Li *et al.*, 2010; Shan *et al.*, 2010; Wils *et al.*, 2010; Xu *et al.*, 2010), which is consistent with our observations in the rat model. In this context, it can be interpreted that the cytoplasmic mislocalization of wild-type TDP-43 is an epiphenomenon and not a necessary condition for the disease. However, in our monkey model, TDP-43 mislocalization was detected in almost all of the large motoneurons of the lateral nuclear group at the early or even the presymptomatic stage, and these motoneurons later showed neuron loss. In contrast, overexpressed exogenous TDP-43 in the large motoneurons of the ventromedial nuclear group was restricted to the nucleus, but did not produce neuron loss. Mice with over-expression of human TDP-43 engineered to localize in the cytoplasm showed progressive neuronal loss and downregulation of endogenous nuclear mouse TDP-43 expression (Igaz *et al.*, 2011). These suggest that TDP-43 mislocalization is an upstream event in the cascade of motoneuronal degeneration. This finding is consistent with the observation that the highest percentage of neurons with TDP-43 mislocalization was found in the early stage of ALS in patients (Giordana *et al.*, 2010).

In conclusion, our monkey model is superior to rodent models in recapitulating the TDP-43 pathology and in the presence of Bunina body-like inclusion and is expected to be a powerful tool for investigating developing effective therapies as well as the disease pathogenesis of sporadic ALS.

Acknowledgements

The authors are grateful to Drs Masato Hasegawa, Makoto Urushitani and Hiroshi Tsukagoshi for discussion and technical advices on Western blotting and pathological analysis; Dr Takashi Shimada, and Ms Fumiko Sunaga for AAV preparation; Dr Satoshi Ikeda, Dr Masumi Ichikawa, Dr Kinya Ishikawa, Miss Tomoko Ueno, Miss Minako Suzuki, Ms Michiko Imanishi, and Ms Hiromi Kondo for technical support on pathological analysis; Dr Kazuo Kusano for surgical support; Ms Yuki Yamamoto, Dr Miho Akaza for their help.

Funding

Comprehensive Research on Disability Health and Welfare (Grant Nos 20301501 and 23161501 to T.Y. and H.M.); Research on Neurodegenerative Diseases/ALS from Ministry of Health, Labor and Welfare, Japan; Grant-in-Aid for Scientific Research (A) (Grant No. 22240039 to T.Y.) and Grant-in-Aid for Research Activity Start-up (Grant No. 22890051 to T.T.) and Strategic Research Program for Brain Science, Field E from Ministry of Education, Culture, Sports and Technology, Japan.

Supplementary material

Supplementary material is available at *Brain* online.

References

Anderson KD, Gunawan A, Steward O. Spinal pathways involved in the control of forelimb motor function in rats. Exp Neurol 2005; 194: 161–74.

Arai T, Hasegawa M, Akiyama H, Ikeda K, Nonaka T, Mori H, et al. TDP-43 is a component of ubiquitin-positive tau-negative inclusions in frontotemporal lobar degeneration and amyotrophic lateral sclerosis. Biochem Biophys Res Commun 2006; 351: 602–11.

Ash PE, Zhang YJ, Roberts CM, Saldi T, Hutter H, Buratti E, et al. Neurotoxic effects of TDP-43 overexpression in *C. elegans*. Hum Mol Genet 2010; 19: 3206–18.

Ayala YM, De Conti L, Avendaño-Vázquez SE, Dhir A, Romano M, D'Ambrogio A, et al. TDP-43 regulates its mRNA levels through a negative feedback loop. EMBO J 2011; 30: 277–88.

Bilsland LG, Sahai E, Kelly G, Golding M, Greensmith L, Schiavo G. Deficits in axonal transport precede ALS symptoms in vivo. Proc Natl Acad Sci USA 2010; 107: 20523–8.

Brooks BR, Miller RG, Swash M, Munsat TL. El Escorial revisited: revised criteria for the diagnosis of amyotrophic lateral sclerosis. Amyotroph Lateral Scler Other Motor Neuron Disord 2000; 1: 293–9.

Buratti E, Baralle FE. Characterization and functional implications of the RNA binding properties of nuclear factor TDP-43, a novel splicing regulator of CFTR exon 9. J Biol Chem 2001; 276: 36337–43.

Buratti E, Baralle FE. Multiple roles of TDP-43 in gene expression, splicing regulation, and human disease. Front Biosci 2008; 13: 867–8.

Buratti E, De Conti L, Stuani C, Romano M, Baralle M, Baralle F. Nuclear factor TDP-43 can affect selected microRNA levels. FEBS J 2010; 277: 2268–81.

Cairns NJ, Neumann M, Bigio EH, Holm IE, Troost D, Hatanpaa KJ, et al. TDP-43 in familial and sporadic frontotemporal lobar degeneration with ubiquitin inclusions. Am J Pathol 2007; 171: 227–40.

Carpenter MB, Sutin J. Human neuroanatomy. 8th edn. Baltimore: Williams & Wilkins; 1983.

Corbo M, Hays AP. Peripherin and neurofilament protein coexist in spinal spheroids of motor neuron disease. J Neuropathol Exp Neurol 1992; 51: 531–7.

De Carvalho M, Dengler R, Eisen A, England JD, Kaji R, Kimura J, et al. Electrodiagnostic criteria for diagnosis of ALS. Clin Neurophysiol 2008; 119: 497–503.

Dengler R, Konstanzer A, Küther G, Hesse S. Amyotrophic lateral sclerosis: Macro-EMG and twitch forces of single motor units. Muscle Nerve 1990; 13: 545–50.

Geser F, Lee VM, Trojanowski JQ. Amyotrophic lateral sclerosis and frontotemporal lobar degeneration: A spectrum of TDP-43 proteinopathies. Neuropathology 2010; 30: 103–12.

Giordana MT, Piccinini M, Grifoni S, De Marco G, Vercellino M, Magistrello M, et al. TDP-43 redistribution is an early event in sporadic amyotrophic lateral sclerosis. Brain Pathol 2010; 20: 351–60.

Gitcho MA, Bigio EH, Mishra M, Johnson N, Weintraub S, Mesulam M, et al. TARDBP 3'-UTR variant in autopsy-confirmed frontotemporal lobar degeneration with TDP-43 proteinopathy. Acta Neuropathol 2009; 11: 633–45.

Hanson KA, Kim SH, Wassarman DA, Tibbetts RS. Ubiquilin modifies TDP-43 toxicity in a Drosophila model of amyotrophic lateral sclerosis (ALS). J Biol Chem 2010; 285: 11068–72.

Harverkamp LJ, Appel V, Appel SH. Natural history of amyotrophic lateral sclerosis in a data base population. Validation of a scoring system and a model for survival prediction. Brain 1995; 118: 707–19.

Hasegawa M, Arai T, Nonaka T, Kametani F, Yoshida M, Hashizume Y, et al. Phosphorylated TDP-43 in frontotemporal lobar degeneration and amyotrophic lateral sclerosis. Ann Neurol 2008; 64: 60–70.

Igaz LM, Kwong LK, Chen-Plotkin A, Winton MJ, Unger TL, Xu Y, et al. Expression of TDP-43 C-terminal fragments in vitro recapitulates pathological features of TDP-43 proteinopathies. J Biol Chem 2009; 284: 8516–24.

Igaz LM, Kwong LK, Lee EB, Chen-Plotkin A, Swanson E, Unger T, et al. Dysregulation of the ALS-associated gene TDP-43 leads to neuronal death and degeneration in mice. J Clin Invest 2011; 121: 726–38.

Kabashi E, Lin L, Tradewell ML, Dion PA, Bercier V, Bourgouin P, et al. Gain and loss of function of ALS-related mutations of TARDBP (TDP-43) cause motor deficits in vivo. Hum Mol Genet 2010; 19: 671–83.

Kabashi E, Valdmanis PN, Dion P, Spiegelman D, McConkey BJ, Vande Velde C, et al. TARDBP mutations in individuals with sporadic and familial amyotrophic lateral sclerosis. Nat Genet 2008; 40: 572–4.

Körner S, Kollewe K, Fahlbusch M, Zapf A, Dengler R, Krampfl K, et al. Onset and spreading patterns of upper and lower motor neuron symptoms in amyotrophic lateral sclerosis. Muscle Nerve 2011; 43: 636–42.

Li Y, Ray P, Rao EJ, Shi C, Guo W, Chen X, et al. A Drosophila model for TDP-43 proteinopathy. Proc Natl Acad Sci USA 2010; 107: 3169–74.

Mackenzie IRA, Neumann M, Baborie A, Sampathu DM, Plessis DD, Jaros E, et al. A harmonized classification system for FTLD-TDP pathology. Acta Neuropathol 2011; 122: 111–3.

Mishra M, Paunesku T, Woloschak GE, Siddique T, Zhu LJ, Lin S, et al. Gene expression analysis of frontotemporal lobar degeneration of the motor neuron disease type with ubiquitinated inclusions. Acta Neuropathol 2007; 114: 81–94.

Mitsumoto H, Chad DA, Pioro EP. Amyotrophic lateral sclerosis. Philadelphia: F.A. Davis; 1998.

Munoz DG, Greene C, Perl DP, Selkoe DJ. Accumulation of phosphorylated neurofilaments in anterior horn motoneurons of amyotrophic lateral sclerosis patients. J Neuropathol Exp Neurol 1988; 47: 9–18.

Neumann M, Kwong LK, Lee EB, Kremmer E, Flatley A, Xu Y, et al. Phosphorylation of S409/410 of TDP-43 is a consistent feature in all sporadic and familial forms of TDP-43 proteinopathies. Acta Neuropathol 2009; 117: 137–49.

Neumann M, Sampathu DM, Kwong LK, Truax AC, Micsenyi MC, Chou TT, et al. Ubiquitinated TDP-43 in frontotemporal lobar degeneration and amyotrophic lateral sclerosis. Science 2006; 314: 130–3.

Okamoto K, Hirai S, Amari M, Watanabe M, Sakurai A. Bunina bodies in amyotrophic lateral sclerosis immunostained with rabbit anti-cystatin C serum. Neurosci Lett 1993; 162: 125–8.

Ou SH, Wu F, Harrich D, Garcia-Martinez LF, Gaynor RB. Cloning and characterization of a novel cellular protein, TDP-43, that binds to human immunodeficiency virus type 1 TAR DNA sequence motifs. J Virol 1995; 69: 3584–96.

Piao YS, Wakabayashi K, Kakita A, Yamada M, Hayashi S, Morita T, et al. Neuropathology with clinical correlations of sporadic amyotrophic lateral sclerosis:102 autopsy cases examined between 1962 and 2000. Brain Pathol 2003; 13: 10–22.

Polymenidou M, Lagier-Tourenne C, Hutt KR, Huelga SC, Moran J, Liang TY, et al. Long pre-mRNA deletion and RNA missplicing contribute to neuronal vulnerability from loss of TDP-43. Nat Neurosci 2011; 14: 459–68.

Pun S, Santos AF, Saxena S, Xu L, Caroni P. Selective vulnerability and pruning of phasic motoneuron axons in motoneuron disease alleviated by CNTF. Nat Neurosci 2006; 9: 408–19.

Shan X, Chiang PM, Price DL, Wong PC. Altered distributions of gemini of coiled bodies and mitochondria in motor neurons of TDP-43 transgenic mice. Proc Natl Acad Sci USA 2010; 107: 16325–30.

Swarup V, Phaneuf D, Bareil C, Robertson J, Rouleau GA, Kriz J, et al. Pathological hallmarks of amyotrophic lateral sclerosis/frontotemporal lobar degeneration in transgenic mice produced with TDP-43 genomic fragments. Brain 2011; 134: 2610–26.

Tan CF, Eguchi H, Tagawa A, Onodera O, Iwasaki T, Tsujino A, et al. TDP-43 immunoreactivity in neuronal inclusions in familial amyotrophic lateral sclerosis with or without SOD1 gene mutation. Acta Neuropathol 2007; 113: 535–42.

Tateishi T, Hokonohara T, Yamasaki R, Miura S, Kikuchi H, Iwaki A, et al. Multiple system degeneration with basophilic inclusions in Japanese ALS patients with FUS mutation. Acta Neuropathol 2010; 119: 355–64.

Voigt A, Herholz D, Fiesel FC, Kaur K, Müller D, Karsten P, et al. TDP-43-mediated neuron loss in vivo requires RNA-binding activity. PLoS ONE 2010; 5: e12247.

Wils H, Kleinberger G, Janssens J, Pereson S, Joris G, Cuijt I, et al. TDP-43 transgenic mice develop spastic paralysis and neuronal inclusions characteristic of ALS and frontotemporal lobar degeneration. Proc Natl Acad Sci USA 2010; 107: 3858–63.

Xu YF, Gendron TF, Zhang YJ, Lin WL, D'Alton S, Sheng H, et al. Wild-type human TDP-43 expression causes TDP-43 phosphorylation, mitochondrial aggregation, motor deficits, and early mortality in transgenic mice. J Neurosci 2010; 30: 10851–9.

Yokoseki A, Shiga A, Tan CF, Tagawa A, Kaneko H, Koyama A, et al. TDP-43 mutation in familial amyotrophic lateral sclerosis. Ann Neurol 2008; 63: 538–42.

Zhang YJ, Xu YF, Cook C, Gendron TF, Roettges P, Link CD, et al. Aberrant cleavage of TDP-43 enhances aggregation and cellular toxicity. Proc Natl Acad Sci USA 2009; 106: 7607–12.

NEUROPATHOLOGY

Neuropathology 2013; **33**, 47–58 doi:10.1111/j.1440-1789.2012.01329.x

Original Article

Neuropathologic analysis of Lewy-related α-synucleinopathy in olfactory mucosa

Sayaka Funabe,[1,4] Masaki Takao,[1] Yuko Saito,[5] Hiroyuki Hatsuta,[1] Mikiko Sugiyama,[1] Shinji Ito,[1] Kazutomi Kanemaru,[2] Motoji Sawabe,[3] Tomio Arai,[3] Hideki Mochizuki,[6] Nobutaka Hattori[4] and Shigeo Murayama[1]

Departments of [1]Neuropathology, [2]Neurology, [3]Pathology, Tokyo Metropolitan Geriatric Hospital and Institute of Gerontology, [4]Department of Neurology, Juntendo University, [5]Department of Laboratory Medicine, National Center Hospital for Neurology and Psychiatry, Tokyo and [6]Department of Neurology, Faculty of Medicine, Osaka University, Osaka, Japan

We analyzed the incidence and extent of Lewy-related α-synucleinopathy (LBAS) in the olfactory mucosa, as well as the central and peripheral nervous systems of consecutive autopsy cases from a general geriatric hospital. The brain and olfactory mucosa were immunohistochemically examined using antibodies raised against phosphorylated α-synuclein. Thirty-nine out of 105 patients (37.1%) showed LBAS in the central or peripheral nervous systems. Seven patients presented LBAS (Lewy neurites) in the olfactory lamina propria mucosa. One out of the seven cases also showed a Lewy neurite in a bundle of axons in the cribriform plate, but α-synuclein deposits were not detected in the olfactory receptor neurons. In particular, high incidence of α-synuclein immunopositive LBAS in the olfactory mucosa was present in the individuals with clinically as well as neuropathologically confirmed Parkinson's disease and dementia with Lewy bodies (6/8 cases, 75%). However, this pathologic alteration was rare in the cases with incidental or subclinical Lewy body diseases (LBD) (one out of 31 cases, 3.2%). In the olfactory bulb, the LBAS was usually present in the glomeruli and granular cells of most symptomatic and asymptomatic cases with LBD. Our studies further confirmed importance of the olfactory entry zone in propagation of LBAS in the human aging nervous system.

Key words: α-synuclein, Lewy body, neuropathology, olfactory mucosa, Parkinson's disease.

Correspondence: Shigeo Murayama, MD, PhD, Department of Neuropathology, Tokyo Metropolitan Geriatric Hospital and Institute of Gerontology, 35-2, Sakae-cho, Itabashi-ku, Tokyo 173-0015, Japan. Email: smurayam@tmig.or.jp

Received 30 March 2012; revised and accepted 19 April 2012; published online 4 June 2012.

INTRODUCTION

Sporadic Parkinson's disease is a neurodegenerative disorder characterized clinically by resting tremor, rigidity, bradykinesia and gait disturbance, as well as neuropathologically by the loss of neurons in several brainstem nuclei and the presence of Lewy bodies formed by abnormal accumulation of α-synuclein.[1–5] Of the many types of neurons in the central and peripheral nervous systems, a specific subset of neurons is vulnerable to accumulation of α-synuclein, which takes the form of aggregates such as Lewy bodies and Lewy neurites (LBs/LNs).[6–8]

Based on studies of a large number of autopsy cases, the initial sites involved in Lewy-related pathology are reported to be the dorsal motor nucleus of the vagus, the intermediate reticular zone in the lower brainstem and olfactory bulb.[9,10] We previously reported that in the earliest stage of Lewy-related α-synucleinopathy (LBAS), abnormal α-synuclein accumulation extends from the peripheral part of the olfactory bulb to the anterior olfactory nucleus as well as the amygdala.[11] From a clinical standpoint, impaired olfactory function constitutes one of the earliest symptoms of sporadic Parkinson's disease.[12,13] Therefore, the olfactory system may be one of the vital regions in the development of Lewy body disease (LBD).

In the olfactory bulb, α-synuclein accumulation is observed in the anterior olfactory nucleus as well as the mitral, tufted, and granular cells of individuals with clinical Parkinson's disease or dementia with Lewy bodies (DLB). Even in the early stages of these diseases, LNs, LBs or both, can be seen in the olfactory bulbs.[11,14,15] Based on the results of a neuropathologic study, Beach *et al.* suggested that the olfactory bulb may be a candidate region of biopsy study to